Glucose starvation and hypoxia, but not the saturated fatty acid palmitic acid or cholesterol, activate the unfolded protein response in 3T3-F442A and 3T3-L1 adipocytes

Adina D. Mihai[1-3] and Martin Schröder[1-3*]

1) Durham University, School of Biological and Biomedical Sciences, Durham DH1 3LE, United Kingdom

2) Biophysical Sciences Institute, Durham University, Durham DH1 3LE, United Kingdom

3) North East England Stem Cell Institute (NESCI), Life Bioscience Centre, International Centre for Life, Central Parkway, Newcastle Upon Tyne, NE1 4EP, United Kingdom

*Address for correspondence: Martin Schröder, Durham University, School of Biological and Biomedical Sciences, Durham DH1 3LE, United Kingdom.

phone: +44 (0) 191-334-1316

FAX: +44 (0) 191-334-9104

email: martin.schroeder@durham.ac.uk

Running Title: ER stress in adipocytes

Keywords: adipocyte, diabetes, glucose starvation, hypoxia, obesity, unfolded protein response

Abstract

Obesity is associated with endoplasmic reticulum (ER) stress and activation of the unfolded protein response (UPR) in adipose tissue. In this study we identify physiological triggers of ER stress and of the UPR in adipocytes *in vitro*. We show that two markers of adipose tissue remodelling in obesity, glucose starvation and hypoxia, cause ER stress in 3T3-F442A and 3T3-L1 adipocytes. Both conditions induced molecular markers of the IRE1α and PERK branches of the UPR, such as splicing of *XBP1* mRNA and CHOP, as well as transcription of the ER stress responsive gene *BiP*. Hypoxia also induced an increase in phosphorylation of the PERK substrate eIF2α. By contrast, physiological triggers of ER stress in many other cell types, such as the saturated fatty acid palmitic acid, cholesterol, or several inflammatory cytokines including TNF-α, IL-1β, and IL-6, do not cause ER stress in 3T3-F442A and 3T3-L1 adipocytes. Our data suggest that physiological changes associated with remodelling of adipose tissue in obesity, such as hypoxia and glucose starvation, are more likely physiologic ER stressors of adipocytes than the lipid overload or hyperinsulinemia associated with obesity.

Introduction

Obesity is the leading risk factor for type 2 diabetes, cardiovascular disease, and hypertension.[1, 2] Obesity affects the homeostasis of the whole body but mainly the liver and the adipose tissue, and is characterized by low grade inflammation, hyperlipidemia, and insulin resistance in surrounding and peripheral tissues.[1, 2] Adipose tissue is exposed to several stresses in obesity, including inflammation, hypoxia, and endoplasmic reticulum (ER) stress.[3] Limited angiogenesis, adipocyte hypertrophy and hyperplasia cause hypoxia in obese adipose tissue.[4] Secretion of MCP-1 by dysfunctional adipocytes attracts circulating monocytes into adipose tissue,[5, 6] while a change in the adipokine profile, including decreased adiponectin and increased leptin secretion,[5] may contribute to the replacement of adipose

41 tissue resident alternatively activated (M2) macrophages with classically activated (M1)
42 macrophages.[6] While physiologic causes of inflammation and hypoxia in adipose tissue have
43 been characterised, little is known about the physiologic triggers of ER stress in obese
44 adipose tissue. At the molecular level, ER stress is caused by the build-up of misfolded
45 proteins in the ER and activation of a signalling network called the unfolded protein response
46 (UPR).[7] The UPR attempts to restore ER homeostasis by inducing expression of genes
47 encoding molecular chaperones and protein foldases, lipid biosynthetic enzymes, and proteins
48 involved in ER-associated protein degradation. If the ER stress cannot be resolved, the UPR
49 promotes apoptosis. ER stress also plays key roles in both inflammation and insulin
50 resistance in obesity and type 2 diabetes.[8, 9]

51 In mammalian cells, three UPR signalling cascades are initiated by the ER
52 transmembrane proteins PERK, IRE1α, and ATF6. Phosphorylation of the translation
53 initiation factor eIF2α by the protein kinase PERK inhibits general translation, but also
54 stimulates translation of mRNAs harbouring several short upstream open reading frames in
55 their 5' untranslated regions. This mechanism of translational activation results in induction
56 of the transcription factors ATF4 and C/EBP homologous protein (CHOP).[10, 11] CHOP
57 reactivates protein synthesis and oxidation in the ER.[12] IRE1α up-regulates ER chaperone
58 genes and genes involved in ER-associated protein degradation via endoribonuclease domain-
59 induced splicing of X-box protein 1 (XBP1) mRNA.[13, 14] The transcription factor ATF6
60 translocates to the nucleus after proteolytic release from the Golgi membrane by the Golgi
61 proteases S1P and S2P[15] and induces expression of genes encoding ER resident molecular
62 chaperones and proteins functioning in ER-associated protein degradation.[16, 17] Upon
63 prolonged or irremediable ER stress the UPR induces apoptosis via activation of JNK[18] by
64 IRE1α and TRB3 by CHOP.[19]

65 The physiological factors leading to ER stress and activation of the UPR in obese
66 adipocytes are not well characterized. For several other cell types, including hepatocytes,
67 pancreatic β cells, and macrophages physiologic ER stressors have been reported. Saturated
68 fatty acids (SFAs) or cholesterol loading induce an UPR in several cell types such as
69 hepatocytes,[20, 21] pancreatic β cells,[22] macrophages,[23] and preadipocytes.[24] Inflammatory
70 cytokines such as TNF-α, IL-6 and IL-1β, which are secreted by stressed adipocytes or
71 macrophages recruited into inflamed adipose tissue,[25] elicit an ER stress response in L929
72 myoblast cells and hepatocytes.[26, 27] Glucose starvation is the earliest identified physiological
73 ER stressor,[28, 29] while the hypoxic environment of tumours induces an UPR in tumour
74 cells.[30-32]

75 The purpose of this study was to identify obesity-related physiological inducers of ER
76 stress and the UPR in adipocytes by exposing *in vitro* differentiated 3T3-F442A adipocytes to
77 several physiologic ER stressors, including the SFA palmitic acid, cholesterol, inflammatory
78 cytokines, glucose starvation, and hypoxia. We report that potent physiologic ER stressors in
79 other cell types, such as palmitic acid, cholesterol, or the inflammatory cytokines TNF-α, IL-
80 1β, and IL-6, do not induce an ER stress response in *in vitro* differentiated 3T3-F442A or
81 3T3-L1 adipocytes. Glucose starvation and hypoxia, however, induce markers of ER stress,
82 such as splicing of *XBP1* mRNA, transcriptional activation of ER stress responsive genes
83 including *BiP*, and *ERDJ4*, CHOP and phosphorylation of eIF2α. Our results suggest that
84 hypoxia and glucose starvation are likely physiologic ER stressors for adipocytes *in vivo*.

85 **Results**

86 *Palmitate does not induce ER stress in adipocytes*

87 To identify which obesity-related physiological factors trigger the UPR in adipocytes we
88 exposed *in vitro* differentiated 3T3-F442A and 3T3-L1 adipocytes to several compounds
89 whose plasma levels are elevated in obesity,[33-39] including palmitic acid, cholesterol, and the

90 inflammatory cytokines TNF-α, IL-1β, and IL-6. 3T3-F442A adipocytes were chosen
91 because these cells form normal adipose tissue without the addition of exogenous inducers
92 when implanted subcutaneously into athymic mice.[40, 41] 3T3-L1 adipocytes were included to
93 provide a second source of adipocytes. Both cell lines were differentiated for 12 d and the
94 percentage of cells with an increased lipid content determined by flow cytometry with the
95 fluorescent lipid probe nile red.[42] Flow cytometry revealed a mean fluorescence increase of
96 3.2 ± 0.2 fold upon differentiation of 3T3-L1 cells (Fig. 1A). In differentiated 3T3-F442A
97 cells two populations with 2.9 ± 0.1 fold and 25 ± 2 fold increases in nile red fluorescence
98 were distinguishable (Fig. 1B). An ~3 fold increase in nile red fluorescence in differentiated
99 3T3-L1 adipocytes and the larger population of differentiated 3T3-F442A adipocytes is in
100 good agreement with previously published increases in nile red fluorescence during
101 differentiation of human adipocytes[43] and adipogenic differentiation of the murine embryonic
102 stem cell line CGR8.[44] Quantitation of the histograms for the nile red fluorescence by
103 constructing the probability distribution for the increase in nile red fluorescence upon
104 differentiation and the constraint that the nile red fluorescence of adipocytes has to be greater
105 by at least two standard deviations of the mean nile red fluorescence of undifferentiated cells
106 than the nile red fluorescence of undifferentiated cells reveals that 72 ± 3 % of the 3T3-L1
107 and 80 ± 1 % of the 3T3-F442A cells acquired a lipid-laden phenotype. These degrees of
108 differentiation are comparable to previously published data.[45]

109 The granularity of cells increases during differentiation into adipocytes because of the
110 accumulation of lipid droplets.[46] This increase in granularity is reflected by an increase in the
111 side scatter of the exciting laser beam[47] and is also seen after differentiation of both 3T3-L1
112 and 3T3-F442A cells for 12 d (Fig. 1C-D). The side scatter of the highly fluorescent 3T3-
113 F442A adipocyte population (≥ 300 A.U. in Fig. 1B) is significantly higher than the side
114 scatter of the weaker fluorescent population (< 300 A. U., Fig. S2), suggesting that the highly

115 fluorescent cells contain more lipid droplets than the weaker fluorescing population. Forward
116 scatter, which is affected by cell size and shape,[47] decreases in 3T3-L1 cells and becomes
117 more heterogeneous in 3T3-F442A cells (Fig. 1E-F). Taken together, these data suggest that
118 the majority of the 3T3-L1 and 3T3-F442A cells have acquired a lipid-laden phenotype 12 d
119 after initiation of adipogenic differentiation.

120 To determine whether palmitic acid causes ER stress in adipocytes *in vitro*, 3T3-L1 and
121 3T3-F442A adipocytes were incubated with different concentrations (0–1 mM) of palmitate
122 complexed to fatty acid-free bovine serum albumin (BSA) for up to 48 h. The activity of the
123 PERK branch of the UPR was assessed by Western blotting for CHOP, while activation of
124 IRE1α was monitored by measuring splicing of *XBP1* mRNA. Exposure of adipocytes to up
125 to 1 mM palmitate for 48 h did not elevate CHOP levels (Fig. 2A-B), induce detectable levels
126 of *XBP1* splicing (Fig. 2C-D, S3-7), or elevate mRNA levels for the ER stress responsive
127 genes *BiP* (Fig. 3A-B), *CHOP* (Fig. 3C-D), or *ERDJ4* (Fig. 3E-F) especially when compared
128 to the large increases in mRNA levels of these genes and CHOP protein levels in
129 thapsigargin-treated adipocytes (Figs. 2A-B and 3). Treatment with palmitate complexed to
130 BSA for 8 or 24 h did also not induce *XBP1* splicing in 3T3-F442A adipocytes (Figs. S5-7).
131 Palmitate did also not affect the viability of 3T3-F442A adipocytes over a period of up to 48
132 h, while incubation with 1 μM thapsigargin, which causes ER stress by depleting ER luminal
133 Ca^{2+} stores,[48] for 48 h decreased viability by ~37% (Fig. 2E). Palmitate did also not inhibit
134 insulin-stimulated AKT serine 473 phosphorylation in 3T3-F442A adipocytes (Fig. 4A),
135 which is consistent with several other reports.[49-56] To validate that our BSA-palmitate
136 complexes induce ER stress, we characterised *XBP1* splicing in undifferentiated
137 preadipocytes exposed to palmitate complexed to BSA. Exposure of preadipocytes to
138 palmitate complexed to BSA induces *XBP1* splicing in these cells.[24] Indeed, palmitate
139 induced *XBP1* splicing in undifferentiated preadipocytes (Figs. 2F and S8) and also inhibited

140 insulin action in these cells (Fig. 4B). Collectively, these results show that the SFA palmitic
141 acid does not induce ER stress in adipocytes.

142 *Cholesterol does not induce an UPR in adipocytes*

143 To characterize whether cholesterol elicits ER stress in adipocytes we exposed differentiated
144 3T3-F442A and 3T3-L1 adipocytes to 100 μg/ml AcLDL for 48 h. AcLDL did not elevate
145 CHOP levels (Fig. 5A-B), induce *XBP1* splicing (Figs. 5C-D and S9A-B), or elevate *BiP* or
146 *CHOP* mRNA levels (Fig. 6). We, therefore, repeated these experiments in the presence of
147 the ACAT inhibitor TMP-153 to inhibit cholesterol esterification and to elevate intracellular
148 free cholesterol levels. After 24 h no changes in expression of CHOP or in *XBP1* splicing
149 were observed (data not shown). 48 h of treatment with AcLDL and TMP-153 did not
150 increase CHOP protein levels (Fig. 5A-B), induce *XBP1* splicing (Fig. 5C-D), or elevate the
151 mRNA levels for *BiP* (Fig. 6A-B) or *CHOP* (Fig. 6C-D). To validate that AcLDL can, in
152 principle, activate the UPR, we repeated these experiments with *in vitro* differentiated THP-1
153 macrophages which are known to develop ER stress in response to cholesterol overloading.[57]
154 In differentiated THP-1 macrophages AcLDL induced *XBP1* splicing both in the presence
155 and absence of TMP-153 (Figs. 5E and S9C). Treatment of THP-1 macrophages with TMP-
156 153 alone also increased *XBP1* splicing ~2.6 fold (Figs. 5E and S9C). These results suggest
157 that exposure of adipocytes to AcLDL does not cause ER stress.

158 *Proinflammatory cytokines do not induce ER stress in adipocytes*

159 To study whether inflammatory cytokines induce ER stress in adipocytes we exposed
160 differentiated 3T3-F442A adipocytes to various concentrations of TNF-α, IL-6, or IL-1β for
161 up to 24 h. Incubation of adipocytes with increasing concentrations of TNF-α for 24 h did not
162 affect the viability of these cells (Fig. 7A), but also failed to induce *XBP1* splicing (Figs. 7B
163 and S10). Various concentrations of IL-6 and IL-1β also failed to induce *XBP1* splicing over
164 a period of 24 h (Figs. 7D-E and S11-12). To validate that the cytokines possess biological

165 activity we characterized activation of the MAPK kinase JNK in preadipocytes. All three
166 cytokines stimulated phosphorylation of JNK (Fig. 7C and F), thus providing evidence that
167 the cytokine preparations we utilised possess biological activity. Taken together, these data
168 suggest that the inflammatory cytokines TNF-α, IL-6, and IL-1β do not cause ER stress in
169 adipocytes.

170 *Glucose starvation induces ER stress in adipocytes*

171 Prolonged exposure of cells to glucose concentrations of <0.2 g/l induces the ER resident
172 chaperones BiP and GRP94,[28, 58] whose expression is controlled by XBP1 and ATF6. To
173 characterize whether glucose starvation, which may be caused by the poor vascularization of
174 the expanding adipose tissue in obesity, can induce ER stress in adipocytes, we maintained *in*
175 *vitro* differentiated 3T3-F442A and 3T3-L1 adipocytes for up to 24 h in serum free medium
176 supplemented with 2 mM L-glutamine but completely lacking glucose. Glutaminolysis serves
177 as an energy source in this medium.[59, 60] Glucose starvation for 24 h induced CHOP potently
178 in both 3T3-F442A and 3T3-L1 adipocytes (Fig. 8A-B). *XBP1* splicing peaked 12 h after
179 induction of glucose starvation (Fig. S13A) and remained elevated for the next 36 h in 3T3-
180 F442A-adipocytes (Figs. 8C-D and S13B). 24 h of glucose starvation also induced *XBP1*
181 splicing in 3T3-L1 adipocytes and elevated the steady-state mRNA levels of *CHOP*, *BiP*, and
182 *ERDJ4*, and, to a lesser extent, *EDEM1* and *VEGFA* mRNAs in 3T3-F442A adipocytes (Fig.
183 8E). Thus, glucose starvation causes ER stress in adipocytes which coincides with increased
184 expression of the pro-angiogenic factor *VEGFA*.

185 *Hypoxia causes ER stress in adipocytes*

186 We characterized whether hypoxia causes ER stress in *in vitro* differentiated 3T3-F442A
187 adipocytes, because hypoxia is another physiological alteration in poorly vascularized obese
188 adipose tissue.[3] *In vitro* differentiated 3T3-F442A adipocytes were cultured in 0.5% O_2 for up
189 to 8 h before protein extraction and characterisation of ER stress markers and the hypoxia

190 marker HIF1α[61] by Western blotting. Hypoxia increased HIF1α levels within 2 h (Fig. 9A-B)
191 and also led to an increase in eIF2α phosphorylation (Fig. 9A-B), *XBP1* splicing (Fig. 9C-D),
192 and *BiP* mRNA levels (Fig. 9E-F). The increases in *XBP1* splicing, *BiP* mRNA levels, and
193 eIF2α phosphorylation, once manifested, persisted throughout the time course of the
194 experiment. Collectively, these data show that hypoxia induces ER stress in adipocytes.

195 **Discussion**

196 We present evidence that glucose starvation and hypoxia (Figs. 8 and 9), but not palmitate
197 (Figs. 2, 3 and S3-7), cholesterol (Figs. 5, 6, and S9), or several inflammatory cytokines (Fig.
198 7 and S10-12) cause ER stress in two *in vitro* adipocyte models, 3T3-F442A and 3T3-L1.
199 These data suggest that the poor vascularization of adipose tissue in obesity causes ER stress
200 in adipocytes, because adipose tissue expansion in obesity leads to formation of poorly
201 vascularized, hypoxic areas.[3, 4] Glucose starvation may contribute to the adverse effects of
202 hypoxia on adipose tissue, because obese adipocytes reach diameters that are comparable to
203 the maximum distance of diffusive glucose supply from a blood vessel.[62-64] The large overlap
204 of the effects of hypoxia and ER stress on adipose tissue, including inflammation,[4] insulin
205 resistance,[65] changes in adiponectin secretion,[66] and increased angiogenesis,[67-69] suggests that
206 ER stress may contribute to or mediate the effects of hypoxia on adipocytes.

207 Our work also suggests that palmitate, cholesterol, and inflammatory cytokines do not
208 elicit an ER stress response in adipocytes. The mRNA expression for two ER stress sensors,
209 IRE1α and PERK, is similar in preadipocytes and adipocytes (Fig. S14), which suggests that
210 increased basal activity of these ER stress signalling pathways cannot explain the protection
211 of adipocytes from palmitate- or cholesterol-induced ER stress. A dominant feature of
212 adipocyte differentiation is the induction of nearly all enzymes of fatty acid and
213 triacylglycerol synthesis, including stearoyl-CoA desaturases and diacylglycerol
214 acyltransferases.[70, 71] Hence, adipocytes may be protected from palmitate-induced ER stress

215 because of their greatly increased ability to dispose of excess palmitate in their triacylglycerol
216 pool.[72] The expansion of the triacylglycerol pool will also increase the storage capacity of
217 adipocytes for cholesterol[73, 74] and thus may explain why cholesterol does not induce ER
218 stress in adipocytes. Increased cholesterol efflux due to increased expression of the
219 cholesterol transporter ABCA1[75, 76] may also contribute to this cholesterol resistance.
220 Induction of several antioxidant enzymes[77-79] and increased NADPH generation[80] may protect
221 adipocytes against ER stress caused by inflammatory cytokines, because these cytokines
222 cause ER stress via production of reactive oxygen species.[27, 81, 82]

223 Our conclusions differ from conclusions drawn in other studies, which suggest that TNF-
224 α,[83] free fatty acids,[84-87] and cholesterol[88] induce ER stress in adipocytes *in vitro*. Koh *et al.*[83]
225 and Jeon *et al*.[85] have reported that TNF-α and palmitate elevate phosphorylation of eIF2α,
226 induce *ATF3* mRNA and activate JNK in 3T3-L1 adipocytes and, on the basis of these
227 changes, concluded that TNF-α and palmitate cause ER stress in adipocytes. eIF2α
228 phosphorylation and the increase in *ATF3* mRNA downstream of eIF2α phosphorylation are
229 controlled by four protein kinases[89] of which only PERK directly responds to ER stress.[90]
230 JNK is activated by many stresses.[91] The absence of an increase in *XBP1* splicing (Figs. 2C-
231 D, 7B, S3-7, and S10), which is a more specific marker for ER stress, suggests that other
232 stresses are responsible for the increase in the stress markers monitored by Koh *et al.*[83] and
233 Jeon *et al.*[85] Kawasaki *et al*.[86] have reported that exposure of 3T3-L1 adipocytes to 50 μg/ml
234 of a free fatty acid mixture derived from human serum induces *XBP1* splicing, *ATF4*, *BiP*,
235 *CHOP*, *EDEM*, *ERDJ4*, and *PDI* mRNAs. Palmitic acid is considered to be the fatty acid
236 with the greatest potential for cell injury,[92] but elicits ER stress, insulin resistance, or cell
237 injury only at much higher concentrations in several cell types (Fig. 2F and refs. 21, 22, 24,
238 93) and does not induce ER stress in 3T3-F442A or 3T3-L1 adipocytes (Figs. 2, 3, and S3-7).
239 Therefore, compounds other than the SFAs present in the fatty acid mixture used by

240 Kawasaki *et al.*[86] seem to be causing ER stress in adipocytes. Jiao *et al.*[87] reported that a
241 mixture of lauric, myristic, oleic, linoleic, and arachidonic acids induces ER stress and
242 potently inhibits insulin-stimulated AKT serine 473 and threonine 308 phosphorylation in *in*
243 *vitro* differentiated 3T3-L1 adipocytes. These results contradict not only our observations
244 (Figs. 2, 3, and S3-7) but also several other papers which have reported that the unsaturated
245 fatty acids oleic and linoleic acid protect cells from the negative effects of SFAs,[94-100] that the
246 medium-chain fatty acids lauric and myristic acid do not induce insulin resistance,[52] and that
247 palmitate does not affect insulin-stimulated AKT phosphorylation in adipocytes.[49-56] Chen e*t*
248 *al.*[88] reported that oxLDL induces BiP and CHOP in 3T3-L1 adipocytes and suggested that
249 intracellular cholesterol overload may be partially responsible for this ER stress response.
250 Both AcLDL and oxLDL are taken up via the scavenger receptor A by adipocytes.[101] We
251 have not observed activation of *XBP1* splicing in 3T3-F442A or 3T3-L1 adipocytes exposed
252 to AcLDL (Figs. 5 and S9), which suggests that an oxidized lipid or oxidized protein
253 component of oxLDL,[102] but not cholesterol, induces ER stress in adipocytes *in vitro*.

254 In conclusion, our work shows that glucose and oxygen deprivation cause ER stress in
255 adipocytes *in vitro*. In obesity, the rapid expansion of the adipose tissue rather than elevated
256 SFAs, cholesterol, or proinflammatory cytokine levels, may be responsible for ER stress in
257 adipocytes. Future work should address whether improved vascularization of obese adipose
258 tissue, either through genetic or pharmacologic means, can mitigate ER stress in this tissue.

259 **Materials and Methods**

260 **Antibodies and reagents.** Antibodies against AKT (cat. no. 4691), phosphoserine 473-AKT
261 (cat. no. 4060), CHOP (cat. no. 2895), phospho-JNK (cat. no. 4668), JNK (cat. no. 9258), and
262 phospho-eIF2α (cat. no. 9721) were purchased from Cell Signaling Technology Inc. The anti-
263 eIF2α antibody (cat. no. sc-11386) was purchased from Santa Cruz Biotechnology Inc., the
264 anti-HIF1α antibody (cat. no. AF1935) from R&D Systems, the anti-GAPDH antibody (cat.

265 no. G8795) and the monoclonal anti-β-actin antibody (cat. no. A2228) from Sigma-Aldrich.
266 The goat anti-rabbit-IgG (H+L)-horseradish peroxidase (HRP)-conjugated secondary
267 antibody (cat. no. 7074S) was bought from Cell Signaling Technology Inc. The goat anti-
268 mouse IgG (H+L)-HRP-conjugated antibody (cat. no. 31432) and the mouse anti-goat IgG
269 (H+L)-HRP-conjugated antibody (cat. no. 31400) were purchased from Thermo Fisher
270 Scientific. Thapsigargin, dexamethasone (cat. no. D4902), 3-isobutyl-1-methylxanthine
271 (IBMX, cat. no. I5879), insulin (cat. no. I0516), palmitic acid (cat. no. P5585), fatty acid free
272 bovine serum albumin (BSA, cat. no. A3803), BSA (cat. no. A2153), and thiazolyl blue
273 tetrazolium bromide (MTT, cat. no. M5655), and 9-diethylamino-5*H*-benzo[α]phenoxazine-
274 5-one (nile red, cat. no. N3013) were purchased from Sigma-Aldrich. TMP-153 was
275 purchased from Enzo Life Sciences. Native human acetylated LDL (cat. no. 5685-3404) was
276 purchased from AbD Serotec, IL-1β (cat. no. RIL1BI) from Thermo Fisher Scientific, IL-6
277 (cat. no. PHC0066) from Life Technologies, and human TNF-α (cat. no. 8902) from Cell
278 Signaling Technology Inc.

279 **Cell culture.** 3T3-L1 murine preadipocytes[103] were obtained from the ATCC and were
280 maintained as subconfluent cultures in Dulbecco's modified Eagle's medium (DMEM)
281 supplemented with 4.5 g/l D-glucose, 2 mM L-glutamine and 10% (v/v) bovine calf serum.
282 3T3-F442A murine preadipocytes[104] were maintained in DMEM supplemented with 4.5 g/l
283 D-glucose, 2 mM L-glutamine and 10% (v/v) foetal bovine serum (FBS). For
284 differentiation,[45] both cell lines were grown to confluence. Two days post-confluency,
285 differentiation was induced by addition of 1 μg/ml insulin, 0.5 mM IBMX, and 0.25 μM
286 dexamethasone to the medium. The cells were maintained in this medium for three days and
287 then for two more days in medium containing 1 μg/ml insulin. After five days of
288 differentiation insulin was omitted from the medium and the cells were maintained for
289 another seven days. In all experiments both 3T3-F442A and 3T3-L1 adipocytes were used 12

290 d after induction of differentiation. The THP-1 human monocytic leukaemia cell line[105] was
291 maintained in RPMI 1640 medium containing 10% (v/v) foetal bovine serum (FBS) and 2
292 mM L-glutamine. The cells were differentiated into macrophages by incubation with 50 nM
293 phorbol-12-myristate 13-acetate (PMA) for 3 d, followed by incubation for 1 d without
294 PMA.[106] Before addition of AcLDL or TMP-153 the cells were serum-starved for 7 h.

295 **Flow cytometry.** Cells were stained with nile red and analysed by flow cytometry essentially
296 as described before.[42] In brief, cells were trypsinised, washed once with DMEM
297 supplemented with 4.5 g/l D-glucose, 2 mM L-glutamine and 10% (v/v) bovine calf serum,
298 and then with phosphate-buffered saline (PBS, 4.3 mM Na_2HPO_4, 1.47 mM KH_2PO_4, 27 mM
299 KCl, 137 mM NaCl, pH 7.4), stained for 5 min with 100 ng/ml nile red in PBS, washed once
300 with PBS and immediately analysed by flow cytometry on a BD FACSCalibur Flow
301 Cytometer (BD Biosciences) at a LO flow rate. For each sample ~50,000 gated events were
302 collected. Nile red fluorescence was excited at 488 nm and its fluorescence emission
303 collected using the FL-1 (530/30 nm) band pass filter set. The instrument settings for 3T3-L1
304 cells were FSC – E-1 (lin, Amp gain = 4.50), SSC – 326 V (lin, Amp gain = 1.00), and FL1 –
305 275 V (log, Amp gain = 1.00), and for 3T3-F442A cells FSC – E-1 (lin, Amp gain = 4.50),
306 SSC – 280 V (lin, Amp gain = 1.00), and FL1 – 275 V (log, Amp gain = 1.00). No thresholds
307 were applied. Data were analysed in WinMDI 2.9 and graphs prepared in GraphPad Prism
308 6.04 (GraphPad Software). Three biological replicates were analysed for each sample and
309 results are represented as the average and standard error of these three repeats.

310 **Cell viability** was determined using the MTT assay.[107] In short, after TNF-α or palmitate
311 treatment cells were incubated for 4 h at 37°C with 0.5 g/l MTT in phenol-red free DMEM
312 containing 4.5 g/l D-glucose, and 2 mM L-glutamine or 2% (w/v) BSA, respectively.
313 Insoluble formazan crystals were dissolved for 15 min in isopropanol containing 4 mM HCl
314 and 0.1% (v/v) Nonidet P-40. The absorbance of the formazan solution was read at a

315 wavelength of 590 nm and a reference wavelength of 620 nm and the formazan absorbance
316 expressed as the ratio of the absorbance at 590 nm to the absorbance at 620 nm.

317 **Palmitate treatment**. *In vitro* differentiated 3T3-F442A adipocytes were serum-starved
318 overnight in DMEM containing 4.5 g/l D-glucose, and 2 mM L-glutamine and then incubated
319 in serum-free medium containing 2% (w/v) fatty acid-free BSA and 0.05-1 mM palmitic acid.
320 These palmitate concentrations are in the physiological range reported for rodents and
321 humans.[108] Palmitic acid was complexed to fatty acid-free BSA as follows. In brief, palmitic
322 acid was dissolved in ethanol and diluted 1:100 in DMEM containing 4.5 g/l D-glucose and
323 2% (w/v) fatty acid-free BSA before addition to the cells. Control cells received ethanol
324 diluted 1:100 into DMEM containing 4.5 g/l D-glucose and 2% (w/v) fatty acid-free BSA.[109]

325 **Cholesterol and cytokine treatments.** *In vitro* differentiated adipocytes were incubated in
326 DMEM containing 4.5 g/l D-glucose, 2 mM L-glutamine, and 100 μg/ml human acetylated
327 LDL (AcLDL) in the presence or absence of the acyl-CoA:cholesterol acyltransferase
328 (ACAT) inhibitor TMP-153 at a final concentration of 0.6 μM. The cells were incubated with
329 cytokines in serum-free medium.

330 **D-Glucose starvation experiments** were performed by incubating the cells for the indicated
331 times in D-glucose-free DMEM supplemented with 2 mM L-glutamine. Control cells '+ D-
332 glucose') were incubated for the same time in DMEM containing 4.5 g/l D-glucose and 2
333 mM L-glutamine.

334 **Hypoxia experiments** were performed using a Billups-Rotenberg hypoxia chamber. A pre-
335 analysed gas mixture of 0.5% (v/v) O_2, 5% (v/v) CO_2 and nitrogen (BOC Industrial Gases)
336 was flushed through the chamber at a flow rate of 25 l/min for 5 min to completely replace air
337 inside the chamber with the gas mixture. The hypoxia chamber was incubated at 37°C for the
338 indicated times. Cells were rapidly harvested and lysed at 4ºC using degassed buffers as
339 described before.[110]

340 **RNA analysis.** RNA was extracted and analysed by reverse transcriptase (RT) PCR as
341 described before.[110] Primers for quantitative PCR (qPCR) are listed in Table 1. RT-qPCR
342 data were standardized to *ACTB* as loading control. The percentage of *XBP1* splicing was
343 calculated by dividing the signal for spliced *XBP1* mRNA by the sums of the signals for
344 spliced and unspliced *XBP1* mRNAs. Band intensities were quantitated using ImageJ.

345 **Protein extraction and Western blotting.** Cells were washed three times with ice-cold PBS
346 and lysed in RIPA buffer [50 mM Tris-HCl, pH 8.0, 150 mM NaCl, 0.5% (w/v) sodium
347 deoxycholate, 0.1% (v/v) Triton X-100, 0.1% (w/v) SDS] containing Roche complete
348 protease inhibitors (cat. no. 11836153001, Roche Applied Science) and phosphatase
349 inhibitors (cat. no. 04 906 837 001, Roche Applied Science) as described before.[110]

350 Proteins were separated by SDS-PAGE on 4-20% Criterion TGX Precast gels (cat. no.
351 567-1094, Bio-Rad Laboratories) and transferred to polyvinylidene difluoride (PVDF)
352 membranes (Amersham HyBond^{TM}-P, pore size 0.45 μm, cat. no. RPN303F, GE Healthcare)
353 by semi-dry electrotransfer in 0.1 M Tris, 0.192 M glycine, and 5% (v/v) methanol at 2
354 mA/cm^2 for 60-75 min. Membranes were then blocked for 1 h in 5% (w/v) skimmed milk
355 powder in TBST [20 mM Tris-HCl, pH 7.6, 137 mM NaCl, and 0.1% (v/v) Tween-20] for
356 antibodies against non-phosphorylated proteins and 5% BSA in TBST for antibodies against
357 phosphorylated proteins. Incubations with antibodies were performed over night at 4°C with
358 gentle agitation. Blots were washed three times with TBST and then probed with secondary
359 antibody for 1 hour at room temperature. The rabbit anti-AKT, anti-phospho-S473-AKT,
360 anti-phospho-S51-eIF2α, anti-JNK and anti-phospho-JNK antibodies were used at a 1:1,000
361 dilution in TBST + 5% (w/v) BSA. The rabbit anti-eIF2α antibody was used at a 1:500
362 dilution in TBST + 5% (w/v) skimmed milk powder. Membranes were developed with goat
363 anti-rabbit-IgG (H+L)-horseradish peroxidase (HRP)-conjugated secondary antibody at a
364 1:1,000 dilution in TBST + 5% (w/v) skimmed milk powder for 1 h at room temperature. The

365 mouse anti-CHOP antibody and anti-β-actin antibodies were used at a 1:1,000 dilution in
366 TBST + 5% (w/v) skimmed milk powder, and the mouse anti-GAPDH antibody at a 1:30,000
367 dilution in TBST + 5% (w/v) skimmed milk powder. These antibodies were developed with
368 goat anti-mouse IgG (H+L)-horseradish peroxidase (HRP)-conjugated secondary antibody at
369 a 1:20,000 dilution in TBST 5% (w/v) skimmed milk powder for 1 h at room temperature.
370 The goat anti-HIF1α antibody was used at a dilution of 1:500 in TBST + 5% (w/v) skimmed
371 milk powder and developed with mouse anti-goat IgG (H+L)-HRP-conjugated antibody at a
372 dilution of 1:30,000 in TBST + 5% (w/v) skimmed milk powder for 1 h at room temperature.
373 To reprobe blots for detection of nonphosphorylated proteins, membranes were stripped using
374 Restore Western Blot Stripping Buffer (Thermo Fisher Scientific, Loughborough, UK, cat.
375 no. 21059) and blocked with 5% (w/v) skimmed milk powder in TBST.

376 For signal detection, Pierce ECL Western Blotting Substrate (cat. no. 32209) or Pierce
377 ECL Plus Western Blotting Substrate (cat. no. 32132) from Thermo Fisher Scientific were
378 used. Blots were exposed to CL-X Posure™ film (cat. no. 34091, Thermo Fisher Scientific).
379 Exposure times were adjusted on the basis of previous exposures to obtain exposures in the
380 linear range of the film. Films were scanned on a CanoScan LiDE 600F scanner (Canon) and
381 saved as tif files. Bands were quantified using ImageJ exactly as described under the heading
382 "Gels Submenu" on the ImageJ web site
383 (http://rsb.info.nih.gov/ij/docs/menus/analyze.html#plot). Peak intensities for the
384 experimental antibody were then divided by the peak intensities obtained with the antibody
385 for the loading control in the corresponding lane to correct for differences in loading between
386 individual lanes. All loading control-corrected peak intensities obtained for one Western blot
387 were then expressed relative to the loading control-corrected peak intensity of the 0 h sample.

388 **Statistical analysis.** All data are presented as the average and standard error of three
389 independently differentiated adipocyte cultures. Errors were propagated using the law of error

390 propagation for random, independent errors.[111] Statistical analyses were performed in
391 GraphPad Prism 6.04. The statistical tests and corrections for multiple comparison used to
392 analyse the data are described in detail in the figure legends.

393 **Acknowledgements**

394 A.D.M. and M.S. devised the study, analysed the data, designed the experiments and wrote
395 the manuscript. This work was supported by Diabetes UK BDA 09/0003949 grant. We thank
396 A. Benham (Durham University) for providing the human THP-1 cells and C. Hutchison
397 (Durham University) for providing the 3T3-F442A preadipocytes. We thank O. Alainis and
398 C. Manning for help with the flow cytometry.

399 **References**
400

401 1. Hotamisligil GS. Inflammation and metabolic disorders. Nature 2006; 444: 860-7.

402 2. Van Gaal LF, Mertens IL, De Block CE. Mechanisms linking obesity with
403 cardiovascular disease. Nature 2006; 444: 875-80.

404 3. Sun K, Kusminski CM, Scherer PE. Adipose tissue remodeling and obesity. J Clin
405 Invest 2011; 121: 2094-101.

406 4. Ye J, Gao Z, Yin J, He Q. Hypoxia is a potential risk factor for chronic inflammation
407 and adiponectin reduction in adipose tissue of *ob/ob* and dietary obese mice. Am J Physiol
408 Endocrinol Metab 2007; 293: E1118-28.

409 5. Coenen KR, Gruen ML, Chait A, Hasty AH. Diet-induced increases in adiposity, but
410 not plasma lipids, promote macrophage infiltration into white adipose tissue. Diabetes 2007;
411 56: 564-73.

412 6. Lumeng CN, Bodzin JL, Saltiel AR. Obesity induces a phenotypic switch in adipose
413 tissue macrophage polarization. J Clin Invest 2007; 117: 175-84.

414 7. Schröder M. Endoplasmic reticulum stress responses. Cell Mol Life Sci 2008; 65:
415 862-94.

416 8. Zhang K, Kaufman RJ. From endoplasmic-reticulum stress to the inflammatory
417 response. Nature 2008; 454: 455-62.
418 9. Samuel VT, Shulman GI. Mechanisms for insulin resistance: Common threads and
419 missing links. Cell 2012; 148: 852-71.
420 10. Gregor MF, Hotamisligil GS. Adipocyte stress: The endoplasmic reticulum and
421 metabolic disease. J Lipid Res 2007; 48: 1905-14.
422 11. Schröder M, Kaufman RJ. ER stress and the unfolded protein response. Mutat Res
423 2005; 569: 29-63.
424 12. Marciniak SJ, Yun CY, Oyadomari S, Novoa I, Zhang Y, Jungreis R, Nagata K,
425 Harding HP, Ron D. CHOP induces death by promoting protein synthesis and oxidation in
426 the stressed endoplasmic reticulum. Genes Dev 2004; 18: 3066-77.
427 13. Calfon M, Zeng H, Urano F, Till JH, Hubbard SR, Harding HP, Clark SG, Ron D.
428 IRE1 couples endoplasmic reticulum load to secretory capacity by processing the *XBP-1*
429 mRNA. Nature 2002; 415: 92-6.
430 14. Yoshida H, Matsui T, Yamamoto A, Okada T, Mori K. XBP1 mRNA is induced by
431 ATF6 and spliced by IRE1 in response to ER stress to produce a highly active transcription
432 factor. Cell 2001; 107: 881-91.
433 15. Ye J, Rawson RB, Komuro R, Chen X, Dave UP, Prywes R, Brown MS, Goldstein
434 JL. ER stress induces cleavage of membrane-bound ATF6 by the same proteases that process
435 SREBPs. Mol Cell 2000; 6: 1355-64.
436 16. Wu J, Rutkowski DT, Dubois M, Swathirajan J, Saunders T, Wang J, Song B, Yau
437 GD-Y, Kaufman RJ. ATF6α optimizes long-term endoplasmic reticulum function to protect
438 cells from chronic stress. Dev Cell 2007; 13: 351-64.

439 17. Yamamoto K, Sato T, Matsui T, Sato M, Okada T, Yoshida H, Harada A, Mori K.
440 Transcriptional induction of mammalian ER quality control proteins is mediated by single or
441 combined action of ATF6α and XBP1. Dev Cell 2007; 13: 365-76.
442 18. Nishitoh H, Matsuzawa A, Tobiume K, Saegusa K, Takeda K, Inoue K, Hori S,
443 Kakizuka A, Ichijo H. ASK1 is essential for endoplasmic reticulum stress-induced neuronal
444 cell death triggered by expanded polyglutamine repeats. Genes Dev 2002; 16: 1345-55.
445 19. Ohoka N, Yoshii S, Hattori T, Onozaki K, Hayashi H. *TRB3*, a novel ER stress-
446 inducible gene, is induced via ATF4-CHOP pathway and is involved in cell death. EMBO J
447 2005; 24: 1243-55.
448 20. Özcan U, Cao Q, Yilmaz E, Lee A-H, Iwakoshi NN, Ozdelen E, Tuncman G, Görgün
449 C, Glimcher LH, Hotamisligil GS. Endoplasmic reticulum stress links obesity, insulin action,
450 and type 2 diabetes. Science 2004; 306: 457-61.
451 21. Wei Y, Wang D, Topczewski F, Pagliassotti MJ. Saturated fatty acids induce
452 endoplasmic reticulum stress and apoptosis independently of ceramide in liver cells. Am J
453 Physiol Endocrinol Metab 2006; 291: E275-81.
454 22. Laybutt DR, Preston AM, Åkerfeldt MC, Kench JG, Busch AK, Biankin AV, Biden
455 TJ. Endoplasmic reticulum stress contributes to beta cell apoptosis in type 2 diabetes.
456 Diabetologia 2007; 50: 752-63.
457 23. DeVries-Seimon T, Li Y, Yao PM, Stone E, Wang Y, Davis RJ, Flavell R, Tabas I.
458 Cholesterol-induced macrophage apoptosis requires ER stress pathways and engagement of
459 the type A scavenger receptor. J Cell Biol 2005; 171: 61-73.
460 24. Guo W, Wong S, Xie W, Lei T, Luo Z. Palmitate modulates intracellular signaling,
461 induces endoplasmic reticulum stress, and causes apoptosis in mouse 3T3-L1 and rat primary
462 preadipocytes. Am J Physiol Endocrinol Metab 2007; 293: E576-86.

463 25. Antuna-Puente B, Feve B, Fellahi S, Bastard J-P. Adipokines: The missing link
464 between insulin resistance and obesity. Diabetes Metab 2008; 34: 2-11.
465 26. Zhang K, Shen X, Wu J, Sakaki K, Saunders T, Rutkowski DT, Back SH, Kaufman
466 RJ. Endoplasmic reticulum stress activates cleavage of CREBH to induce a systemic
467 inflammatory response. Cell 2006; 124: 587-99.
468 27. Xue X, Piao J-H, Nakajima A, Sakon-Komazawa S, Kojima Y, Mori K, Yagita H,
469 Okumura K, Harding H, Nakano H. Tumor necrosis factor α (TNFα) induces the unfolded
470 protein response (UPR) in a reactive oxygen species (ROS)-dependent fashion, and the UPR
471 counteracts ROS accumulation by TNFα. J Biol Chem 2005; 280: 33917-25.
472 28. Shiu RP, Pouyssegur J, Pastan I. Glucose depletion accounts for the induction of two
473 transformation-sensitive membrane proteins in Rous sarcoma virus-transformed chick
474 embryo fibroblasts. Proc Natl Acad Sci U S A 1977; 74: 3840-4.
475 29. Lin AY, Lee AS. Induction of two genes by glucose starvation in hamster fibroblasts.
476 Proc Natl Acad Sci U S A 1984; 81: 988-92.
477 30. Romero-Ramirez L, Cao H, Nelson D, Hammond E, Lee A-H, Yoshida H, Mori K,
478 Glimcher LH, Denko NC, Giaccia AJ, et al. XBP1 is essential for survival under hypoxic
479 conditions and is required for tumor growth. Cancer Res 2004; 64: 5943-7.
480 31. Koumenis C, Naczki C, Koritzinsky M, Rastani S, Diehl A, Sonenberg N, Koromilas
481 A, Wouters BG. Regulation of protein synthesis by hypoxia via activation of the endoplasmic
482 reticulum kinase PERK and phosphorylation of the translation initiation factor eIF2α. Mol
483 Cell Biol 2002; 22: 7405-16.
484 32. Bi MX, Naczki C, Koritzinsky M, Fels D, Blais J, Hu NP, Harding H, Novoa I, Varia
485 M, Raleigh J, et al. ER stress-regulated translation increases tolerance to extreme hypoxia and
486 promotes tumor growth. EMBO J 2005; 24: 3470-81.

487 33. Hotamisligil GS, Arner P, Caro JF, Atkinson RL, Spiegelman BM. Increased adipose
488 tissue expression of tumor necrosis factor-α in human obesity and insulin resistance. J Clin
489 Invest 1995; 95: 2409-15.
490 34. Kern PA, Ranganathan S, Li C, Wood L, Ranganathan G. Adipose tissue tumor
491 necrosis factor and interleukin-6 expression in human obesity and insulin resistance. Am J
492 Physiol Endocrinol Metab 2001; 280: E745-51.
493 35. Misaki Y, Miyauchi R, Mochizuki K, Takabe S, Shimada M, Ichikawa Y, Goda T.
494 Plasma interleukin-1β concentrations are closely associated with fasting blood glucose levels
495 in healthy and preclinical middle-aged nonoverweight and overweight Japanese men.
496 Metabolism 2010; 59: 1465-71.
497 36. Spranger J, Kroke A, Möhlig M, Hoffmann K, Bergmann MM, Ristow M, Boeing H,
498 Pfeiffer AFH. Inflammatory cytokines and the risk to develop type 2 diabetes: Results of the
499 prospective population-based European Prospective Investigation into Cancer and Nutrition
500 (EPIC)-Potsdam Study. Diabetes 2003; 52: 812-7.
501 37. Tremblay AJ, Després JP, Piché ME, Nadeau A, Bergeron J, Alméras N, Tremblay A,
502 Lemieux S. Associations between the fatty acid content of triglyceride, visceral adipose tissue
503 accumulation, and components of the insulin resistance syndrome. Metabolism 2004; 53:
504 310-7.
505 38. Sorensen TI, Andersen B, Kam-Hansen L. Total plasma cholesterol in obesity after
506 jejunoileal bypass with 3:1 or 1:3 jejunoileal ratio. A randomized trial. Scand J Gastroenterol
507 1979; 14: 865-8.
508 39. Dobrea GM, Wieland RG, Johnson MW. The effect of rapid weight loss due to
509 jejunoileal bypass on total cholesterol and high-density lipoprotein. Am J Clin Nutr 1981; 34:
510 1994-6.

511 40. Green H, Kehinde O. Formation of normally differentiated subcutaneous fat pads by
512 an established preadipose cell line. J Cell Physiol 1979; 101: 169-71.
513 41. Mandrup S, Loftus TM, MacDougald OA, Kuhajda FP, Lane MD. Obese gene
514 expression at *in vivo* levels by fat pads derived from s.c. implanted 3T3-F442A
515 preadipocytes. Proc Natl Acad Sci U S A 1997; 94: 4300-5.
516 42. Greenspan P, Mayer EP, Fowler SD. Nile red: A selective fluorescent stain for
517 intracellular lipid droplets. J Cell Biol 1985; 100: 965-73.
518 43. Crandall DL, Quinet EM, Morgan GA, Busler DE, McHendry-Rinde B, Kral JG.
519 Synthesis and secretion of plasminogen activator inhibitor-1 by human preadipocytes. J Clin
520 Endocrinol Metab 1999; 84: 3222-7.
521 44. Schaedlich K, Knelangen JM, Santos AN, Fischer B. A simple method to sort ESC-
522 derived adipocytes. Cytometry A 2010; 77: 990-5.
523 45. Rubin CS, Hirsch A, Fung C, Rosen OM. Development of hormone receptors and
524 hormonal responsiveness *in vitro*. Insulin receptors and insulin sensitivity in the preadipocyte
525 and adipocyte forms of 3T3-L1 cells. J Biol Chem 1978; 253: 7570-8.
526 46. Lee YH, Chen SY, Wiesner RJ, Huang YF. Simple flow cytometric method used to
527 assess lipid accumulation in fat cells. J Lipid Res 2004; 45: 1162-7.
528 47. Rothe G. Technical background and methodological principles of flow cytometry. In:
529 Sack U, Tárnok A, Rothe G, eds. Cellular Diagnostics Basics, Methods and Clinical
530 Applications of Flow Cytometry. Basel: Karger, 2009:53-88.
531 48. Back SH, Schröder M, Lee K, Zhang K, Kaufman RJ. ER stress signaling by
532 regulated splicing: IRE1/HAC1/XBP1. Methods 2005; 35: 395-416.
533 49. Yang L, Qian Z, Ji H, Yang R, Wang Y, Xi L, Sheng L, Zhao B, Zhang X. Inhibitory
534 effect on protein kinase Cθ by crocetin attenuates palmitate-induced insulin insensitivity in
535 3T3-L1 adipocytes. Eur J Pharmacol 2010; 642: 47-55.

536 50. Dasgupta S, Bhattacharya S, Biswas A, Majumdar SS, Mukhopadhyay S, Ray S,
537 Bhattacharya S. NF-κB mediates lipid-induced fetuin-A expression in hepatocytes that
538 impairs adipocyte function effecting insulin resistance. Biochem J 2010; 429: 451-62.
539 51. Xi L, Qian Z, Xu G, Zhou C, Sun S. Crocetin attenuates palmitate-induced insulin
540 insensitivity and disordered tumor necrosis factor-α and adiponectin expression in rat
541 adipocytes. Br J Pharmacol 2007; 151: 610-7.
542 52. Chavez JA, Summers SA. Characterizing the effects of saturated fatty acids on insulin
543 signaling and ceramide and diacylglycerol accumulation in 3T3-L1 adipocytes and C2C12
544 myotubes. Arch Biochem Biophys 2003; 419: 101-9.
545 53. Usui I, Haruta T, Takata Y, Iwata M, Uno T, Takano A, Ueno E, Ishibashi O, Ishihara
546 H, Wada T, et al. Differential effects of palmitate on glucose uptake in rat-1 fibroblasts and
547 3T3-L1 adipocytes. Horm Metab Res 1999; 31: 546-52.
548 54. Hunnicutt JW, Hardy RW, Williford J, McDonald JM. Saturated fatty acid-induced
549 insulin resistance in rat adipocytes. Diabetes 1994; 43: 540-5.
550 55. Van Epps-Fung M, Williford J, Wells A, Hardy RW. Fatty acid-induced insulin
551 resistance in adipocytes. Endocrinology 1997; 138: 4338-45.
552 56. Lundgren M, Eriksson JW. No *in vitro* effects of fatty acids on glucose uptake,
553 lipolysis or insulin signaling in rat adipocytes. Horm Metab Res 2004; 36: 203-9.
554 57. Tao J-L, Ruan X-Z, Li H, Li X-M, Moorhead JF, Varghese Z, Li X-W. Endoplasmic
555 reticulum stress is involved in acetylated low-density lipoprotein induced apoptosis in THP-1
556 differentiated macrophages. Chin Med J (Engl) 2009; 122: 1794-9.
557 58. Kasambalides EJ, Lanks KW. Effects of low molecular weight nutrients on the pattern
558 of proteins synthesized by non-proliferating murine L cells. Exp Cell Res 1981; 132: 31-9.
559 59. Kowalchuk JM, Curi R, Newsholme EA. Glutamine metabolism in isolated incubated
560 adipocytes of the rat. Biochem J 1988; 249: 705-8.

561 60. Yoo H, Antoniewicz MR, Stephanopoulos G, Kelleher JK. Quantifying reductive
562 carboxylation flux of glutamine to lipid in a brown adipocyte cell line. J Biol Chem 2008;
563 283: 20621-7.
564 61. Semenza GL. HIF-1: Mediator of physiological and pathophysiological responses to
565 hypoxia. J Appl Physiol 2000; 88: 1474-80.
566 62. Kallinowski F, Runkel S, Fortmeyer HP, Förster H, Vaupel P. L-glutamine: a major
567 substrate for tumor cells in vivo? J Cancer Res Clin Oncol 1987; 113: 209-15.
568 63. Chandramouli V, Carter JR, Jr. Metabolic effects of 2-deoxy-D-glucose in isolated fat
569 cells. Biochim Biophys Acta 1977; 496: 278-91.
570 64. Skurk T, Alberti-Huber C, Herder C, Hauner H. Relationship between adipocyte size
571 and adipokine expression and secretion. J Clin Endocrinol Metab 2007; 92: 1023-33.
572 65. Yin J, Gao Z, He Q, Zhou D, Guo Z, Ye J. Role of hypoxia in obesity-induced
573 disorders of glucose and lipid metabolism in adipose tissue. Am J Physiol Endocrinol Metab
574 2009; 296: E333-42.
575 66. Hosogai N, Fukuhara A, Oshima K, Miyata Y, Tanaka S, Segawa K, Furukawa S,
576 Tochino Y, Komuro R, Matsuda M, et al. Adipose tissue hypoxia in obesity and its impact on
577 adipocytokine dysregulation. Diabetes 2007; 56: 901-11.
578 67. Michailidou Z, Turban S, Miller E, Zou X, Schrader J, Ratcliffe PJ, Hadoke PW,
579 Walker BR, Iredale JP, Morton NM, et al. Increased angiogenesis protects against adipose
580 hypoxia and fibrosis in metabolic disease-resistant 11β-hydroxysteroid dehydrogenase type 1
581 (HSD1)-deficient mice. J Biol Chem 2012; 287: 4188-97.
582 68. Sung H-K, Doh K-O, Son JE, Park JG, Bae Y, Choi S, Nelson SM, Cowling R, Nagy
583 K, Michael IP, et al. Adipose vascular endothelial growth factor regulates metabolic
584 homeostasis through angiogenesis. Cell Metab 2013; 17: 61-72.

585 69. Sun K, Wernstedt Asterholm I, Kusminski CM, Bueno AC, Wang ZV, Pollard JW,
586 Brekken RA, Scherer PE. Dichotomous effects of VEGF-A on adipose tissue dysfunction.
587 Proc Natl Acad Sci U S A 2012; 109: 5874-9.
588 70. Cornelius P, MacDougald OA, Lane MD. Regulation of adipocyte development.
589 Annu Rev Nutr 1994; 14: 99-129.
590 71. Gregoire FM, Smas CM, Sul HS. Understanding adipocyte differentiation. Physiol
591 Rev 1998; 78: 783-809.
592 72. Bosma M, Dapito DH, Drosatos-Tampakaki Z, Huiping-Son N, Huang L-S, Kersten
593 S, Drosatos K, Goldberg IJ. Sequestration of fatty acids in triglycerides prevents endoplasmic
594 reticulum stress in an in vitro model of cardiomyocyte lipotoxicity. Biochim Biophys Acta
595 2014.
596 73. Kovanen PT, Nikkilä EA, Miettinen TA. Regulation of cholesterol synthesis and
597 storage in fat cells. J Lipid Res 1975; 16: 211-23.
598 74. Prattes S, Hörl G, Hammer A, Blaschitz A, Graier WF, Sattler W, Zechner R, Steyrer
599 E. Intracellular distribution and mobilization of unesterified cholesterol in adipocytes:
600 Triglyceride droplets are surrounded by cholesterol-rich ER-like surface layer structures. J
601 Cell Sci 2000; 113: 2977-89.
602 75. Ross SE, Erickson RL, Gerin I, DeRose PM, Bajnok L, Longo KA, Misek DE, Kuick
603 R, Hanash SM, Atkins KB, et al. Microarray analyses during adipogenesis: understanding the
604 effects of Wnt signaling on adipogenesis and the roles of liver X receptor α in adipocyte
605 metabolism. Mol Cell Biol 2002; 22: 5989-99.
606 76. Burton GR, Nagarajan R, Peterson CA, McGehee RE, Jr. Microarray analysis of
607 differentiation-specific gene expression during 3T3-L1 adipogenesis. Gene 2004; 329: 167-
608 85.

609 77. Higuchi M, Dusting GJ, Peshavariya H, Jiang F, Hsiao ST, Chan EC, Liu GS.
610 Differentiation of human adipose-derived stem cells into fat involves reactive oxygen species
611 and Forkhead box O1 mediated upregulation of antioxidant enzymes. Stem Cells Dev 2013;
612 22: 878-88.

613 78. Qiang L, Farmer SR. C/EBPα-dependent induction of glutathione *S*-transferase
614 ζ/maleylacetoacetate isomerase (GSTζ/MAAI) expression during the differentiation of
615 mouse fibroblasts into adipocytes. Biochem Biophys Res Commun 2006; 340: 845-51.

616 79. Jowsey IR, Smith SA, Hayes JD. Expression of the murine glutathione *S*-transferase
617 α3 (GSTA3) subunit is markedly induced during adipocyte differentiation: Activation of the
618 *GSTA3* gene promoter by the pro-adipogenic eicosanoid 15-deoxy-$\Delta^{12,14}$-prostaglandin J_2.
619 Biochem Biophys Res Commun 2003; 312: 1226-35.

620 80. Si Y, Yoon J, Lee K. Flux profile and modularity analysis of time-dependent
621 metabolic changes of de novo adipocyte formation. Am J Physiol Endocrinol Metab 2007;
622 292: E1637-46.

623 81. Oyadomari S, Takeda K, Takiguchi M, Gotoh T, Matsumoto M, Wada I, Akira S,
624 Araki E, Mori M. Nitric oxide-induced apoptosis in pancreatic β cells is mediated by the
625 endoplasmic reticulum stress pathway. Proc Natl Acad Sci U S A 2001; 98: 10845-50.

626 82. Chambers KT, Unverferth JA, Weber SM, Wek RC, Urano F, Corbett JA. The role of
627 nitric oxide and the unfolded protein response in cytokine induced β-cell death. Diabetes
628 2008; 57: 124-32.

629 83. Koh EH, Park J-Y, Park H-S, Jeon MJ, Ryu JW, Kim M, Kim SY, Kim M-S, Kim S-
630 W, Park IS, et al. Essential role of mitochondrial function in adiponectin synthesis in
631 adipocytes. Diabetes 2007; 56: 2973-81.

632 84. Alhusaini S, McGee K, Schisano B, Harte A, McTernan P, Kumar S, Tripathi G.
633 Lipopolysaccharide, high glucose and saturated fatty acids induce endoplasmic reticulum

634 stress in cultured primary human adipocytes: Salicylate alleviates this stress. Biochem
635 Biophys Res Commun 2010; 397: 472-8.
636 85. Jeon MJ, Leem J, Ko MS, Jang JE, Park H-S, Kim HS, Kim M, Kim EH, Yoo HJ,
637 Lee C-H, et al. Mitochondrial dysfunction and activation of iNOS are responsible for the
638 palmitate-induced decrease in adiponectin synthesis in 3T3L1 adipocytes. Exp Mol Med
639 2012; 44: 562-70.
640 86. Kawasaki N, Asada R, Saito A, Kanemoto S, Imaizumi K. Obesity-induced
641 endoplasmic reticulum stress causes chronic inflammation in adipose tissue. Sci Rep 2012; 2:
642 799.
643 87. Jiao P, Ma J, Feng B, Zhang H, Alan Diehl J, Eugene Chin Y, Yan W, Xu H. FFA-
644 induced adipocyte inflammation and insulin resistance: Involvement of ER stress and IKKβ
645 pathways. Obesity (Silver Spring) 2011; 19: 483-91.
646 88. Chen Y, Chen M, Wu Z, Zhao S. Ox-LDL induces ER stress and promotes the
647 adipokines secretion in 3T3-L1 adipocytes. PLoS One 2013; 8: e81379.
648 89. Dever TE, Chen JJ, Barber GN, Cigan AM, Feng L, Donahue TF, London IM, Katze
649 MG, Hinnebusch AG. Mammalian eukaryotic initiation factor 2α kinases functionally
650 substitute for *GCN2* protein kinase in the *GCN4* translational control mechanism of yeast.
651 Proc Natl Acad Sci U S A 1993; 90: 4616-20.
652 90. Harding HP, Zhang Y, Ron D. Protein translation and folding are coupled by an
653 endoplasmic-reticulum-resident kinase. Nature 1999; 397: 271-4.
654 91. Kyriakis JM, Banerjee P, Nikolakaki E, Dai T, Rubie EA, Ahmad MF, Avruch J,
655 Woodgett JR. The stress-activated protein kinase subfamily of c-Jun kinases. Nature 1994;
656 369: 156-60.
657 92. Li LO, Klett EL, Coleman RA. Acyl-CoA synthesis, lipid metabolism and
658 lipotoxicity. Biochim Biophys Acta 2010; 1801: 246-51.

659 93. Hassan RH, Hainault I, Vilquin J-T, Samama C, Lasnier F, Ferré P, Foufelle F,
660 Hajduch E. Endoplasmic reticulum stress does not mediate palmitate-induced insulin
661 resistance in mouse and human muscle cells. Diabetologia 2012; 55: 204-14.
662 94. Weigert C, Brodbeck K, Staiger H, Kausch C, Machicao F, Haring HU, Schleicher
663 ED. Palmitate, but not unsaturated fatty acids, induces the expression of interleukin-6 in
664 human myotubes through proteasome-dependent activation of nuclear factor-κB. J Biol
665 Chem 2004; 279: 23942-52.
666 95. Miller TA, LeBrasseur NK, Cote GM, Trucillo MP, Pimentel DR, Ido Y, Ruderman
667 NB, Sawyer DB. Oleate prevents palmitate-induced cytotoxic stress in cardiac myocytes.
668 Biochem Biophys Res Commun 2005; 336: 309-15.
669 96. Diakogiannaki E, Welters HJ, Morgan NG. Differential regulation of the endoplasmic
670 reticulum stress response in pancreatic β-cells exposed to long-chain saturated and
671 monounsaturated fatty acids. J Endocrinol 2008; 197: 553-63.
672 97. Katsoulieris E, Mabley JG, Samai M, Green IC, Chatterjee PK. α-Linolenic acid
673 protects renal cells against palmitic acid lipotoxicity via inhibition of endoplasmic reticulum
674 stress. Eur J Pharmacol 2009; 623: 107-12.
675 98. Akazawa Y, Cazanave S, Mott JL, Elmi N, Bronk SF, Kohno S, Charlton MR, Gores
676 GJ. Palmitoleate attenuates palmitate-induced Bim and PUMA up-regulation and hepatocyte
677 lipoapoptosis. J Hepatol 2010; 52: 586-93.
678 99. Salvadó L, Coll T, Gómez-Foix AM, Salmerón E, Barroso E, Palomer X, Vázquez-
679 Carrera M. Oleate prevents saturated-fatty-acid-induced ER stress, inflammation and insulin
680 resistance in skeletal muscle cells through an AMPK-dependent mechanism. Diabetologia
681 2013; 56: 1372-82.

682 100. Sommerweiß D, Gorski T, Richter S, Garten A, Kiess W. Oleate rescues INS-1E β-
683 cells from palmitate induced apoptosis by preventing activation of the unfolded protein
684 response. Biochem Biophys Res Commun 2013; 441: 770-6.
685 101. Steinberg D. Low density lipoprotein oxidation and its pathobiological significance. J
686 Biol Chem 1997; 272: 20963-6.
687 102. Schroepfer GJ, Jr. Oxysterols: Modulators of cholesterol metabolism and other
688 processes. Physiol Rev 2000; 80: 361-554.
689 103. Green H, Kehinde O. Sublines of mouse 3T3 cells that accumulate lipid. Cell 1974; 1:
690 113-6.
691 104. Green H, Kehinde O. Spontaneous heritable changes leading to increased adipose
692 conversion in 3T3 cells. Cell 1976; 7: 105-13.
693 105. Tsuchiya S, Yamabe M, Yamaguchi Y, Kobayashi Y, Konno T, Tada K.
694 Establishment and characterization of a human acute monocytic leukemia cell line (THP-1).
695 Int J Cancer 1980; 26: 171-6.
696 106. Daigneault M, Preston JA, Marriott HM, Whyte MK, Dockrell DH. The identification
697 of markers of macrophage differentiation in PMA-stimulated THP-1 cells and monocyte-
698 derived macrophages. PLoS One 2010; 5: e8668.
699 107. Mosmann T. Rapid colorimetric assay for cellular growth and survival: Application to
700 proliferation and cytotoxicity assays. J Immunol Methods 1983; 65: 55-63.
701 108. Bradley RL, Fisher FF, Maratos-Flier E. Dietary fatty acids differentially regulate
702 production of TNF-α and IL-10 by murine 3T3-L1 adipocytes. Obesity (Silver Spring) 2008;
703 16: 938-44.
704 109. Chavez JA, Knotts TA, Wang LP, Li G, Dobrowsky RT, Florant GL, Summers SA. A
705 role for ceramide, but not diacylglycerol, in the antagonism of insulin signal transduction by
706 saturated fatty acids. J Biol Chem 2003; 278: 10297-303.

707 110. Cox DJ, Strudwick N, Ali AA, Paton AW, Paton JC, Schröder M. Measuring
708 signaling by the unfolded protein response. Methods Enzymol 2011; 491: 261-92.
709 111. Ku HH. Notes on use of propagation of error formulas. J Res Nat Bureau Standards
710 Sect C - Eng Instrumentat 1966; 70: 263-73.
711 112. Dunnett CW. New tables for multiple comparisons with control. Biometrics 1964; 20:
712 482-91.
713 113. Dunnett CW. A multiple comparison procedure for comparing several treatments with
714 a control. J Am Stat Assoc 1955; 50: 1096-121.

715 **Figure legends**

716 **Figure 1. Adipocyte differentiation of 3T3-L1 and 3T3-F442A cells. (A, B)** Nile red
717 fluorescence, **(C, D)** side scatter (SSC-H), and **(E, F)** forward scatter (FSC-H) of (A, C, E)
718 3T3-L1 and (B, D, F) 3T3-F442A cells before (0 d, grey lines) and 12 d after induction of
719 adipocyte differentiation (black lines). The light grey lines represent the autofluorescence of
720 cells differentiated for 12 d. Dot plots of the side scatter SSC-H versus the forward scatter
721 SSC-H for 3T3-L1 and 3T3-F442A cells before and 12 d after differentiation are shown in
722 Fig. S1. The mean nile red fluorescence of preadipocytes is significantly different from the
723 mean nile red fluorescence of differentiated adipocytes in a one way analysis of variance
724 (ANOVA) test with Dunnett's correction for multiple comparisons[112, 113] ($p < 0.0001$ for both
725 3T3-L1 and 3T3-F442A cells).

726 **Figure 2. Palmitate does not induce CHOP protein expression or *XBP1* splicing in**
727 **adipocytes. (A, B)** CHOP expression in *in vitro* differentiated (A) 3T3-F442A adipocytes
728 and (B) 3T3-L1 adipocytes exposed to the indicated concentrations of palmitate complexed to
729 BSA for 48 h. Relative (rel.) CHOP signals were corrected for the loading controls GAPDH
730 or β-actin. The bar graphs show the average and standard error of three independent repeats.
731 Differences are not statistically significant ($p = 0.42$ for 3T3-F442A adipocytes and $p = 0.10$

732 for 3T3-L1 adipocytes in a repeated measures ANOVA test that compares the treated samples
733 to the untreated sample. Equal variabilities of the differences were assumed for the treated
734 and untreated samples and Dunnett's correction for multiple comparisons[112, 113] was used). 1
735 μM thapsigargin (Tg) was used as a positive control for induction of ER stress. Thapsigargin-
736 treated samples were compared to untreated samples using a two-tailed, unpaired *t*-test. **(C,**
737 **D)** *XBP1* splicing in *in vitro* differentiated (C) 3T3-F442A adipocytes and (D) 3T3-L1
738 adipocytes incubated for 48 h with the indicated concentrations of BSA-complexed palmitate.
739 % splicing indicates the percentage of spliced *XBP1* mRNA, for which the average and
740 standard error of three independent experiments are shown. Abbreviations: u – unspliced
741 *XBP1* mRNA, s – spliced *XBP1* mRNA. **(E)** MTT assay on *in vitro* differentiated 3T3-F442A
742 adipocytes incubated for 48 h with the indicated concentrations of BSA-complexed palmitate.
743 A repeated measures ANOVA test was used to compare the treated samples to the untreated
744 sample. Equal variabilities of the differences were assumed for the treated and untreated
745 samples and Dunnett's correction for multiple comparisons[112, 113] was applied. **(F)** *XBP1*
746 splicing in 3T3-F442A preadipocytes incubated for 12 h with the indicated concentrations of
747 BSA-complexed palmitate. Abbreviations: * - $p < 0.05$, ** - $p < 0.0$, *** - $p < 0.001$, and
748 **** - $p < 0.0001$.

749 **Figure 3. Palmitate does not induce *BiP*, *CHOP*, or *ERDJ4* transcription in adipocytes.**
750 **(A, B)** *BiP* mRNA, **(C, D)** *CHOP* mRNA, and **(E, F)** *ERDJ4* mRNA levels in *in vitro*
751 differentiated (A, C, E) 3T3-F442A and (B, D, F) 3T3-L1 adipocytes incubated for 48 h with
752 the indicated concentrations of BSA-complexed palmitate. The differences in *BiP* mRNA (p
753 $= 0.10$ for 3T3-F442A adipocytes and $p = 0.34$ for 3T3-L1 adipocytes), *CHOP* mRNA ($p =$
754 0.11 for 3T3-F442A adipocytes and $p = 0.41$ for 3T3-L1 adipocytes), and *ERDJ4* mRNA (p
755 $= 0.48$ for 3T3-F442A adipocytes and $p = 0.41$ for 3T3-L1 adipocytes) levels in the untreated
756 and palmitate treated samples are not statistically significant. A repeated measures ANOVA

757 test with Dunnett's correction for multiple comparisons[112, 113] and assuming equal
758 variabilities of the differences was used to compare the palmitate-treated samples to the
759 untreated sample. Thapsigargin-treated samples were compared to untreated samples using a
760 two-tailed, unpaired *t*-test.

761 **Figure 4. Palmitate does not inhibit insulin signalling in 3T3-F442A adipocytes. (A)**
762 Serum-starved 3T3-F442A adipocytes and **(B)** serum-starved undifferentiated 3T3-F442A
763 cells were treated with the indicated concentrations of BSA-complexed palmitic acid for 48 h
764 before stimulation with 100 nM insulin for 15 min. Phosphorylation of AKT at serine 473
765 and total AKT levels were determined by Western blotting.

766 **Figure 5. Cholesterol loading does not induce CHOP protein expression or *XBP1***
767 **splicing in adipocytes**. **(A, B)** CHOP protein levels and **(C, D)** *XBP1* splicing in *in vitro*
768 differentiated (A, C) 3T3-F442A and (B, D) 3T3-L1 adipocytes incubated for 48 h with
769 human acetylated LDL (AcLDL), AcLDL and 0.6 μM of the ACAT inhibitor TMP-153, 0.6
770 μM TMP-153, 1.0 μM Tg, or left untreated ('-'). The average and standard error of three
771 independent experiments are shown in the bar graphs. Differences in CHOP protein levels
772 between the untreated sample and the samples treated with AcLDL, AcLDL and 0.6 μM
773 TMP-153, and 0.6 μM TMP-153 are not statistically significant (p = 0.26 for 3T3-F442A
774 adipocytes and p = 0.35 for 3T3-L1 adipocytes in a repeated measures ANOVA test with
775 Dunnett's correction for multiple comparisons[112, 113] comparing the treated samples to the
776 untreated samples and assuming equal variabilities of the differences). **(E)** *XBP1* splicing in
777 untreated *in vitro* differentiated human THP-1 macrophages and macrophages incubated for
778 16 h with AcLDL, AcLDL + 0.6 μM TMP-153, 0.6 μM TMP-153, or 1.0 μM Tg.

779 **Figure 6. Cholesterol loading does not induce *BiP* or *CHOP* transcription in adipocytes**.
780 **(A, B)** *BiP* mRNA and **(C, D)** *CHOP* mRNA levels in *in vitro* differentiated (A, C) 3T3-
781 F442A and (B, D) 3T3-L1 adipocytes incubated for 48 h with human acetylated LDL

782 (AcLDL), AcLDL and 0.6 μM of the ACAT inhibitor TMP-153, 0.6 μM TMP-153, 1.0 μM
783 Tg, or left untreated ('-'). The average and standard error of three independent experiments
784 are shown. Differences are not statistically significant (*BiP* mRNA: $p = 0.34$ for 3T3-F442A
785 adipocytes and $p = 0.11$ for 3T3-L1 adipocytes; *CHOP* mRNA: $p = 0.09$ for 3T3-F442A
786 adipocytes and $p = 0.11$ for 3T3-L1 adipocytes). p values were obtained from a repeated
787 measures ANOVA test comparing the samples treated with AcLDL, AcLDL and 0.6 μM
788 TMP-153, and 0.6 μM TMP-153 to the untreated samples and assuming equal variabilities of
789 the differences. Dunnett's correction for multiple comparisons[112, 113] was applied.
790 Thapsigargin-treated samples were compared to untreated samples using a two-tailed,
791 unpaired *t*-test.

792 **Figure 7. The proinflammatory cytokines TNF-α, IL-6, and IL-1β do not induce ER**
793 **stress in adipocytes**. **(A)** MTT assay on *in vitro* differentiated 3T3-F442A adipocytes
794 incubated for 24 h with the indicated concentrations of TNF-α. A repeated measures ANOVA
795 test was used to compare the treated samples to the untreated sample. Equal variabilities of
796 the differences were assumed for the treated and untreated samples and Dunnett's correction
797 for multiple comparisons[112, 113] was applied. **(B)** *XBP1* splicing in *in vitro* differentiated 3T3-
798 F442A adipocytes incubated for 24 h with the indicated concentrations of TNF-α or 1.0 μM
799 Tg. The average and standard error from three independent experiments are shown. **(C)** JNK
800 phosphorylation in 3T3-F442A preadipocytes incubated for 30 min with 25 ng/ml TNF-α. **(D**
801 and **E)** *XBP1* splicing in *in vitro* differentiated 3T3-F442A adipocytes incubated for 24 h with
802 the indicated concentrations of (D) IL-6 and (E) IL-1β. The average and standard error of two
803 independent experiments are shown. **(F**) JNK phosphorylation in 3T3-F442A preadipocytes
804 incubated for the indicated times with 200 ng/ml IL-6 or 200 ng/ml IL-1β.

805 **Figure 8. Glucose starvation induces ER stress in adipocytes**. **(A)** CHOP protein levels in
806 *in vitro* differentiated 3T3-F442A and 3T3-L1 adipocytes maintained for 24 h in the presence

807 of 4.5 g/l D-glucose ('+ Glucose') or without any glucose ('- Glucose'). β-Actin was used as
808 a loading control. **(B)** Quantitation of the Western blots shown in panel (A). **(C)** *XBP1*
809 splicing in *in vitro* differentiated 3T3-F442A and 3T3-L1 adipocytes maintained for 24 h in
810 the presence of 4.5 g/l D-glucose or without any glucose. Below the images of the agarose
811 gels the intensity of the ethidium bromide fluorescence was plotted versus the migration
812 distance of the PCR products. (D) Quantitation of XBP1 splicing shown in panel (C). For
813 both cell lines the average and standard error of three independent repeats are shown. **(E)**
814 Steady-state mRNA levels of *CHOP*, *BiP*, *ERDJ4*, *EDEM1, and VEGFA* mRNAs in 3T3-
815 F442A adipocytes maintained for 24 h in the presence of 4.5 g/l D-glucose or without any
816 glucose. *p* values were obtained from two-tailed, unpaired *t*-tests.

817 **Figure 9. Hypoxia induces ER stress in adipocytes**. **(A-B)** Induction of HIF1α and
818 increased phosphorylation of eIF2α at serine 51 in *in vitro* differentiated (A) 3T3-F442A and
819 (B) 3T3-L1 adipocytes incubated for the indicated times under 0.5% (v/v) O_2. **(C-D)** *XBP1*
820 splicing in *in vitro* differentiated (C) 3T3-F442A and (D) 3T3-L1 adipocytes incubated for
821 the indicated times under 0.5% (v/v) O_2. Representative gels from three biological repeats are
822 shown. **(E, F)** Steady-state *BiP* mRNA levels in *in vitro* differentiated 3T3-F442A (E) and
823 3T3-L1 (F) adipocytes incubated for the indicated times under 0.5% (v/v) O_2 were
824 determined by RT-qPCR. *p* values were obtained from a repeated measures ANOVA test
825 comparing the treated samples to the untreated samples and assuming equal variabilities of
826 the differences. Dunnett's correction for multiple comparisons[112, 113] was employed.

827

828 **Table 1. Oligodeoxynucleotides.** The HUGO Gene Nomenclature Committee gene names
829 are given in brackets where these deviate from the commonly used gene names.

Name	Purpose	Sequence
H7961	*XBP1* PCR, forward primer	GATCCTGACGAGGTTCCAGA
H7962	*XBP1* PCR, reverse primer	ACAGGGTCCAACTTGTCCAG
H7994	*ACTB* PCR and RT-qPCR, forward primer	AGCCATGTACGTAGCCATCC
H7995	*ACTB* PCR and RT-qPCR, reverse primer	CTCTCAGCTGTGGTGGTGAA
H8553	*BiP* (*HSPA5*) RT-qPCR, forward primer	TTCGTGTCTCCTCCTGAC
H8554	*BiP* (*HSPA5*) RT-qPCR, reverse primer	ACAGTGAACTTCATCATGCC
H8660	*VEGFA* RT-qPCR, forward primer	AGAGCAACATCACCATGCAG
H8661	*VEGFA* RT-qPCR, reverse primer	TTTGACCCTTTCCCTTTCCT
H8736	*ERDJ4* (*DNAJB9*) RT-qPCR, forward primer	CTGTGGCCCTGACTTGGGTT
H8737	*ERDJ4* (*DNAJB9*) RT-qPCR, reverse primer	AGGGGCAAACAGCCAAAAGC
H8778	*CHOP* RT-qPCR, forward primer	TCTTGAGCCTAACACGTCGAT
H8779	*CHOP* RT-qPCR, reverse primer	CGTGGACCAGGTTCTGCTTT
H8796	*EDEM1* RT-qPCR, forward primer	TGGAAAGCTTCTTTCTCAGC
H8797	*EDEM1* RT-qPCR, reverse primer	ATTCCCGAAGACGTTTGTCC
H9106	*PERK* RT-qPCR, forward primer	CTCAAGTTTCCTCTACTGTTCACTC
H9107	*PERK* RT-qPCR, reverse primer	GCTGTCTCAGAACCGTTTTCCC
H9110	*IRE1α* RT-qPCR, forward primer	GCGCAAATTCAGAACCTACAAAGG
H9111	*IRE1α* RT-qPCR, reverse primer	GGAAGCGGGAAGTGAAGTAGC

830

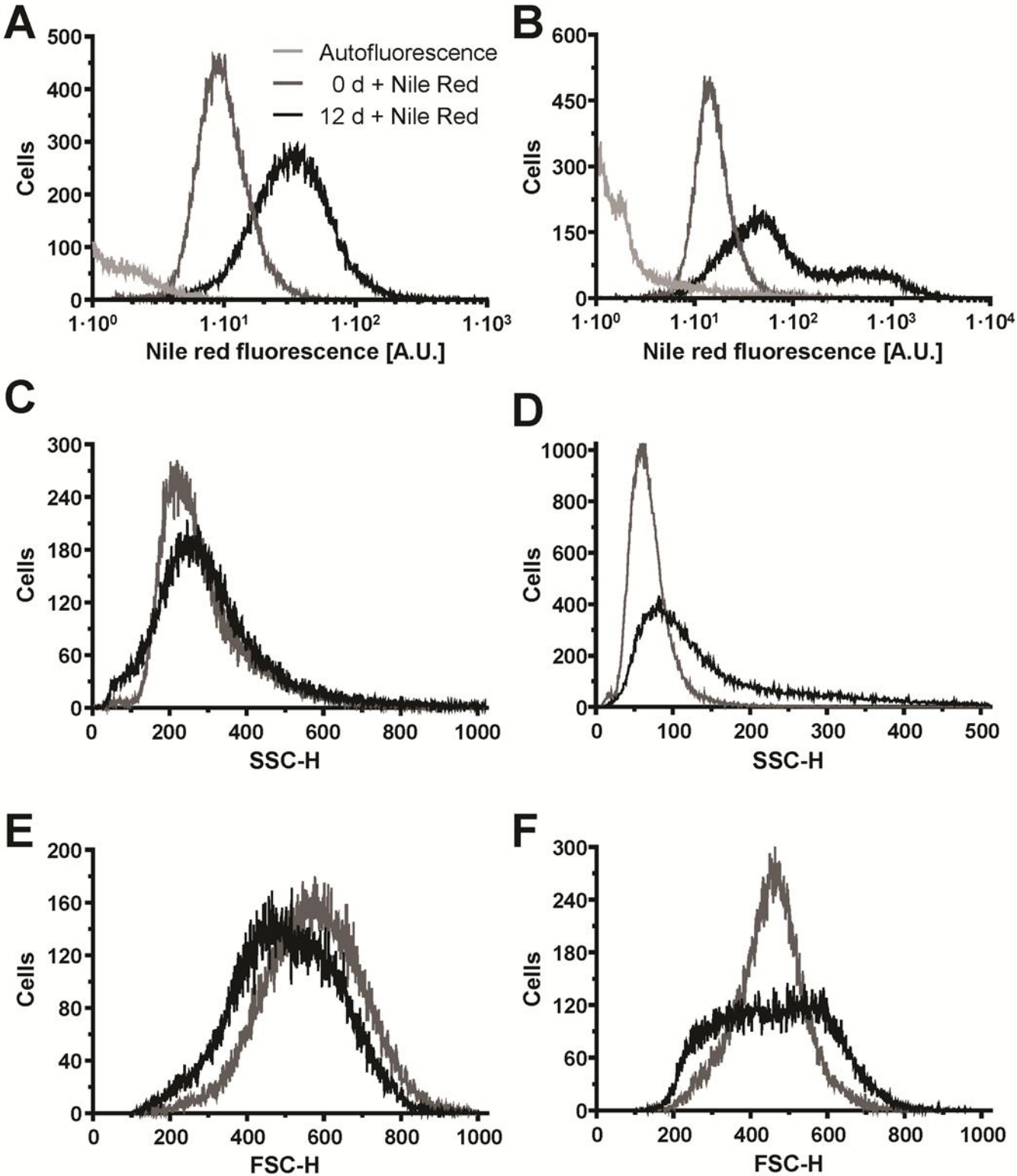

Mihai and Schröder, Figure 1

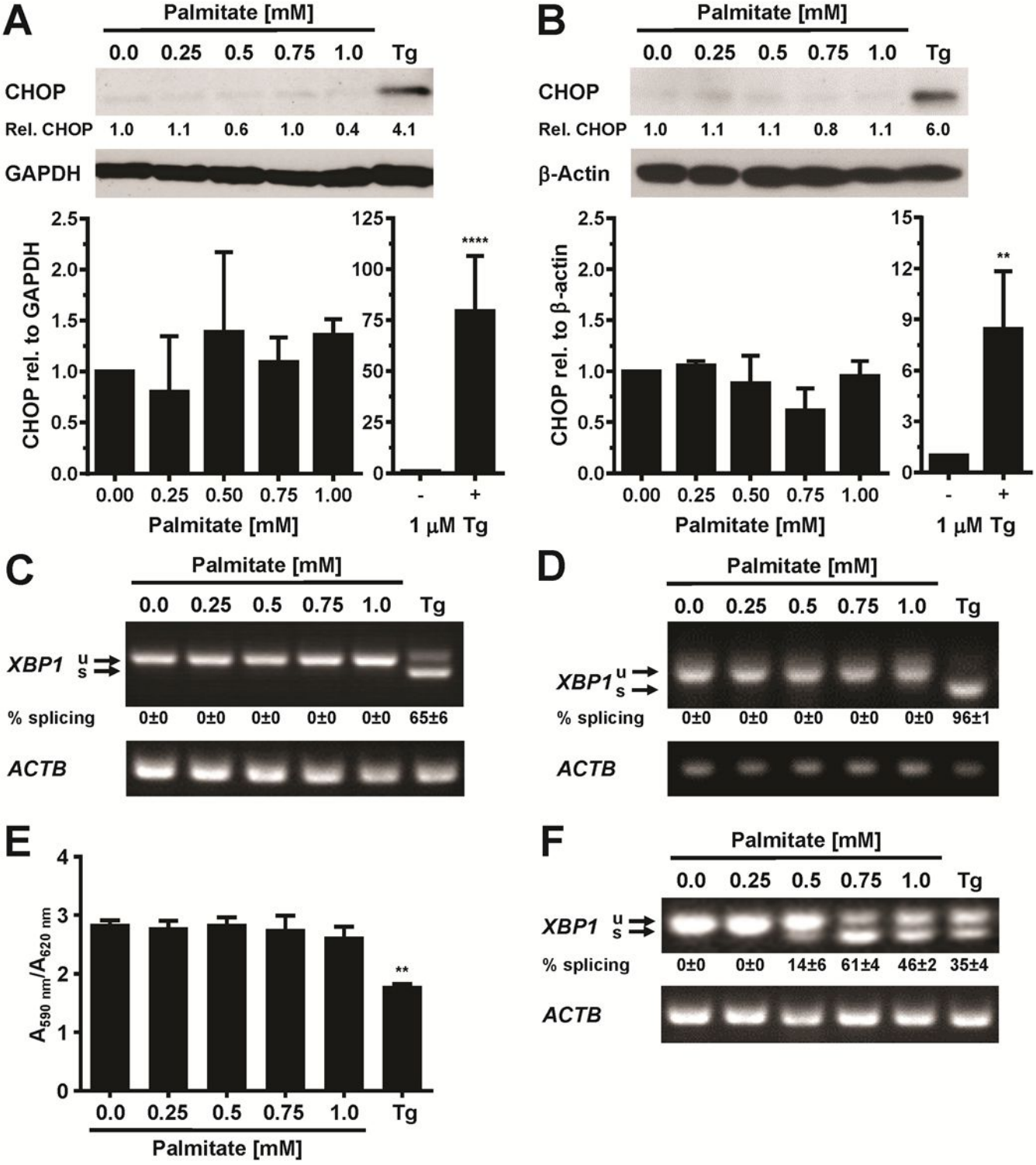

Mihai and Schröder, Figure 2

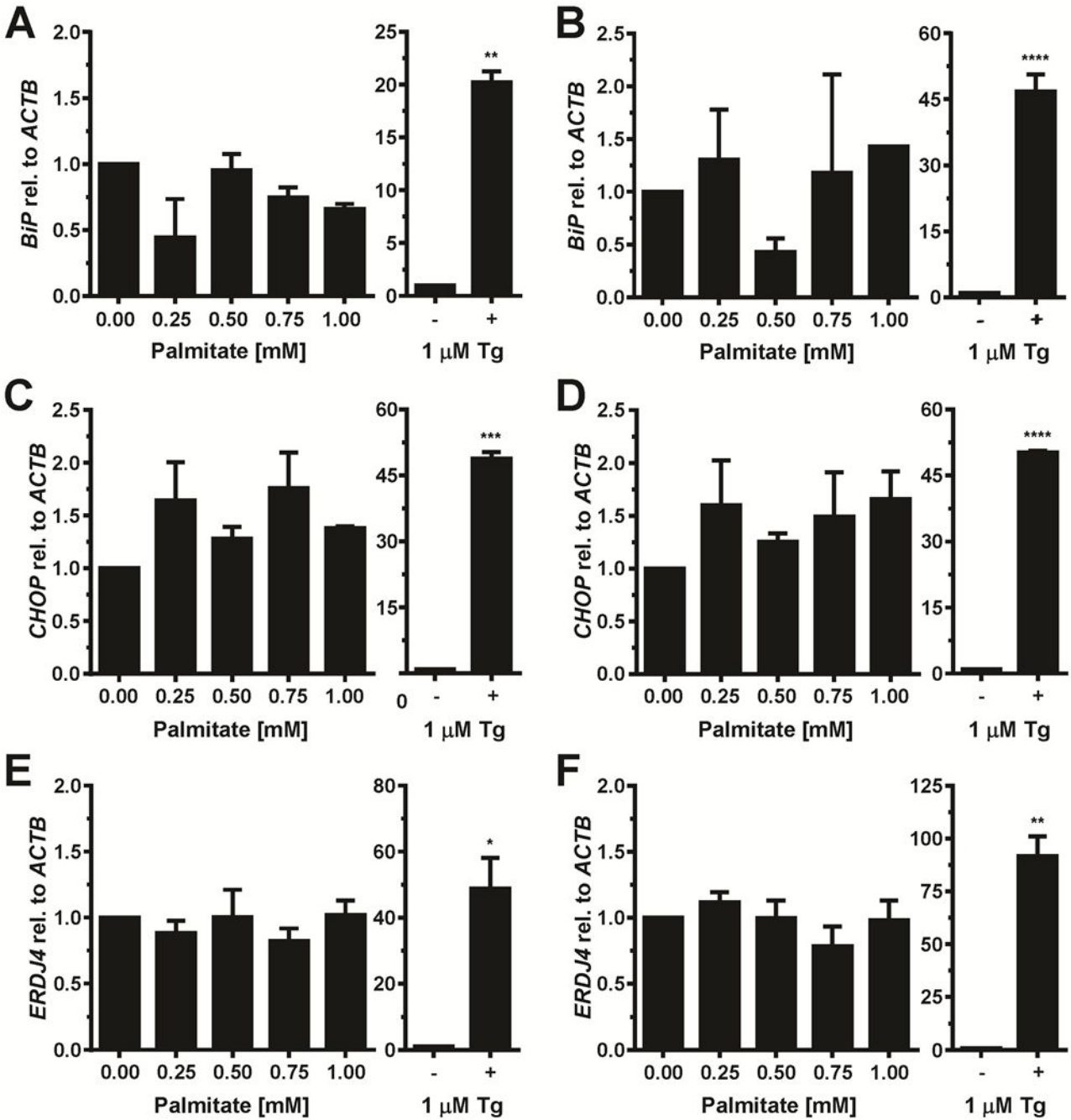

Mihai and Schröder, Figure 3

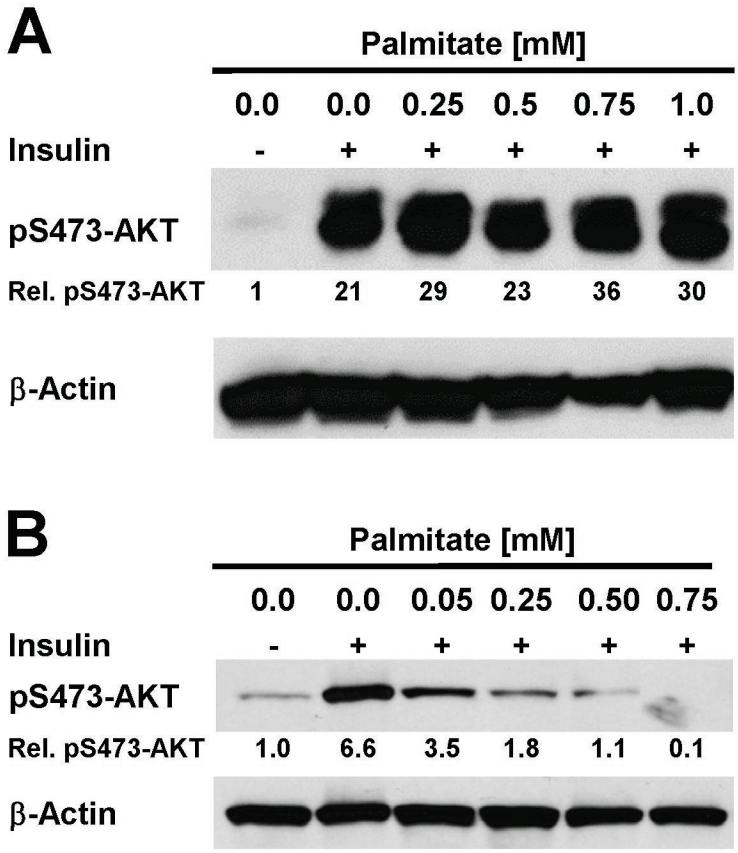

Mihai and Schröder, Figure 4

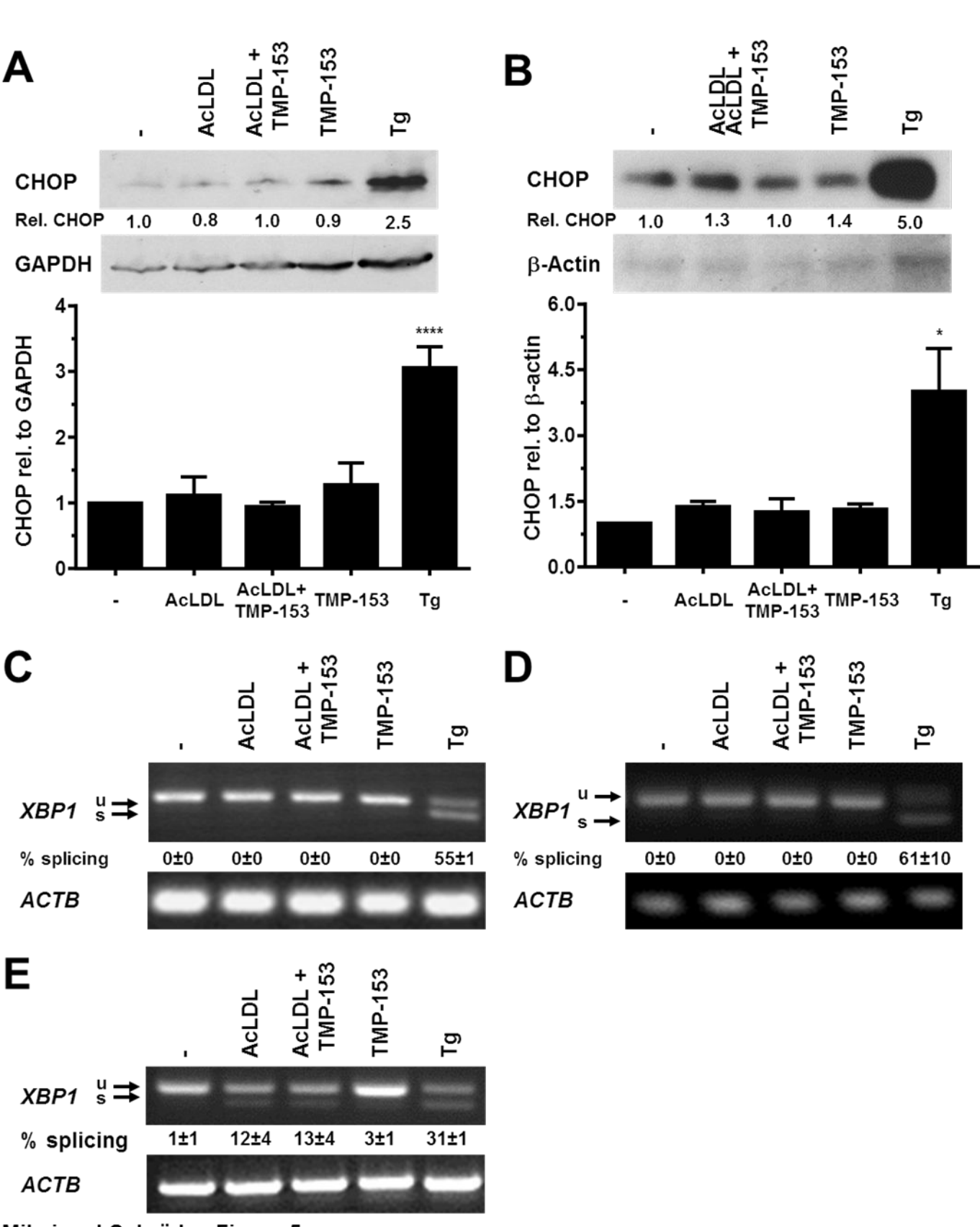

Mihai and Schröder, Figure 5

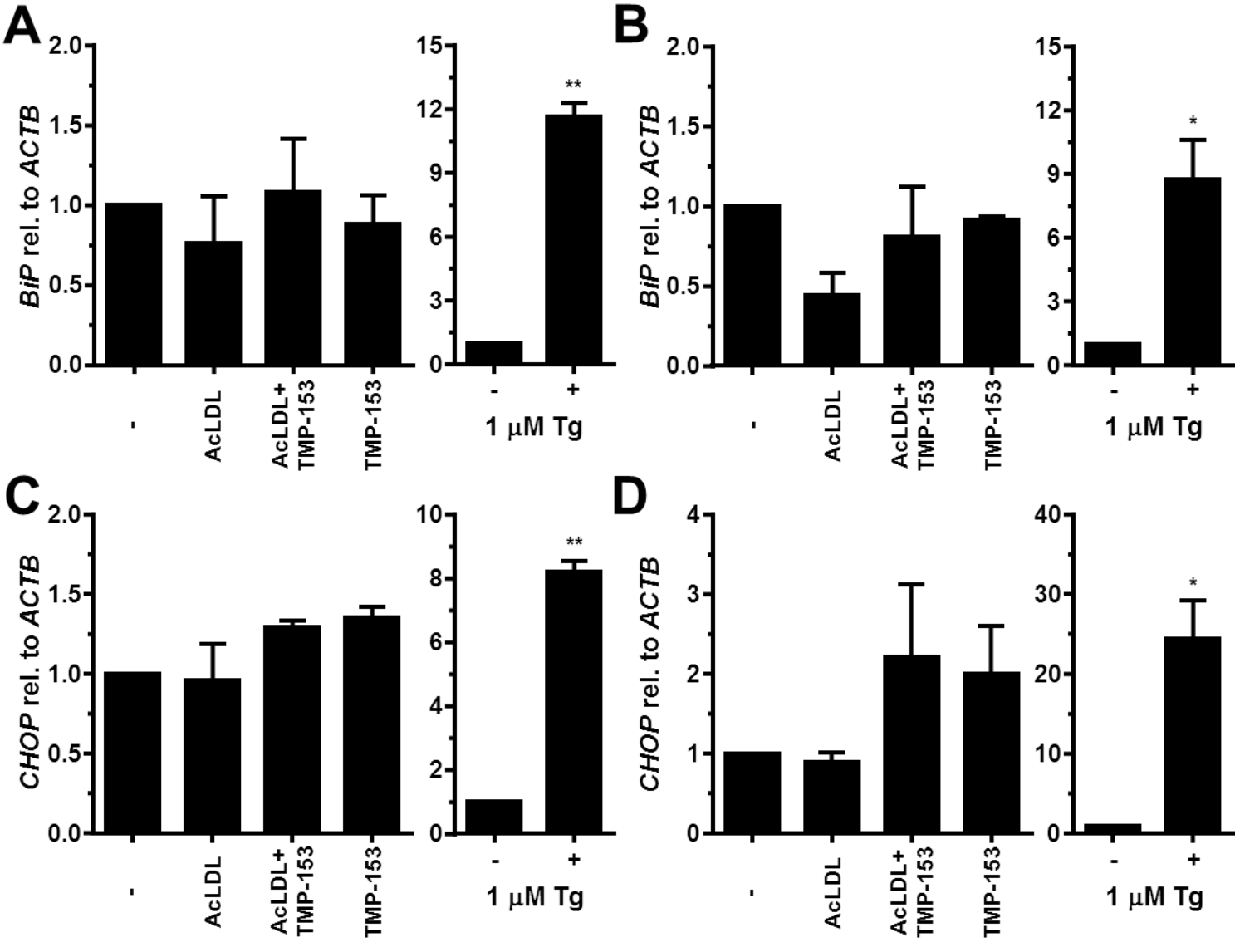

Mihai and Schröder, Figure 6

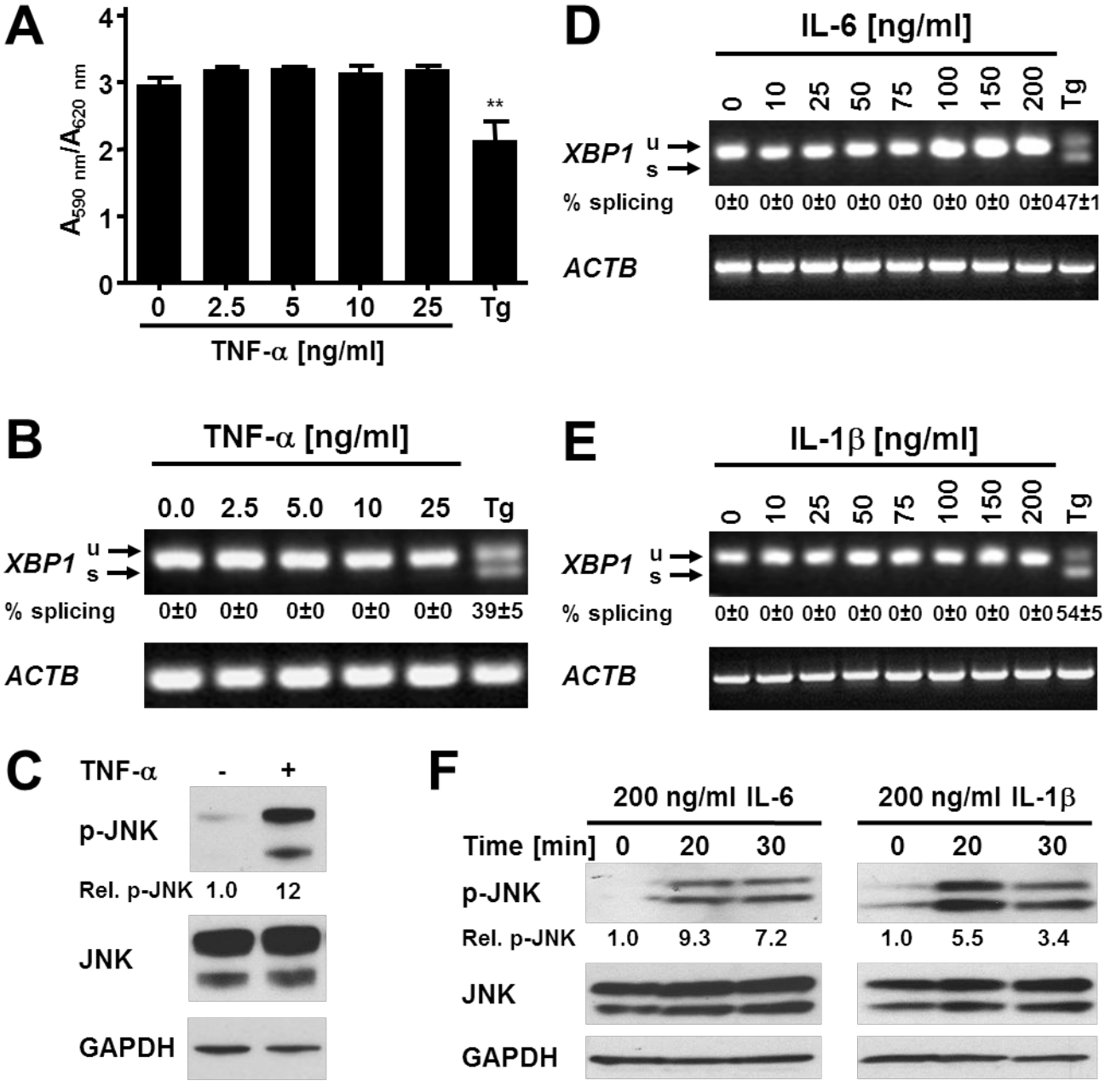

Mihai and Schröder, Figure 7

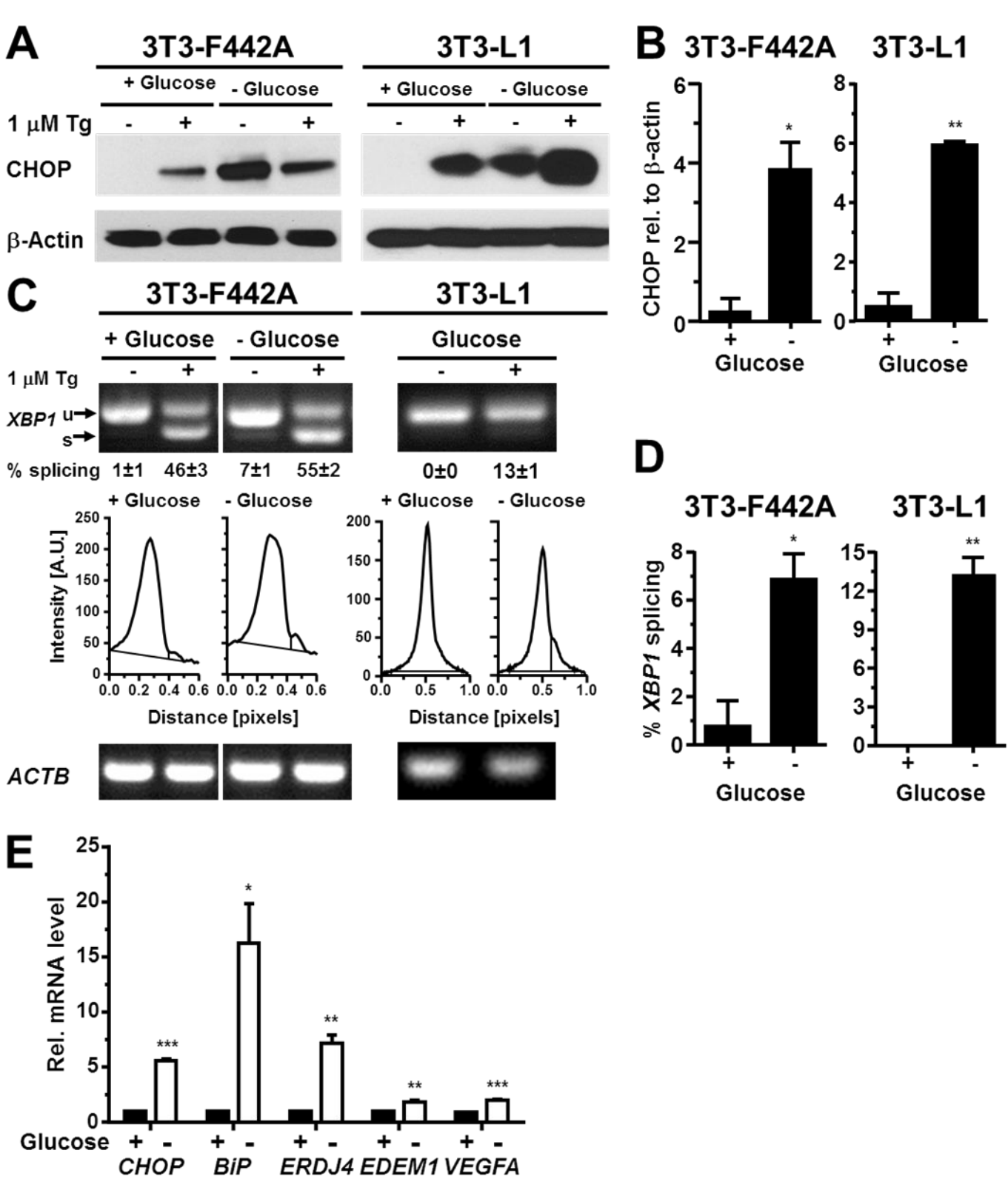

Mihai and Schröder, Figure 8

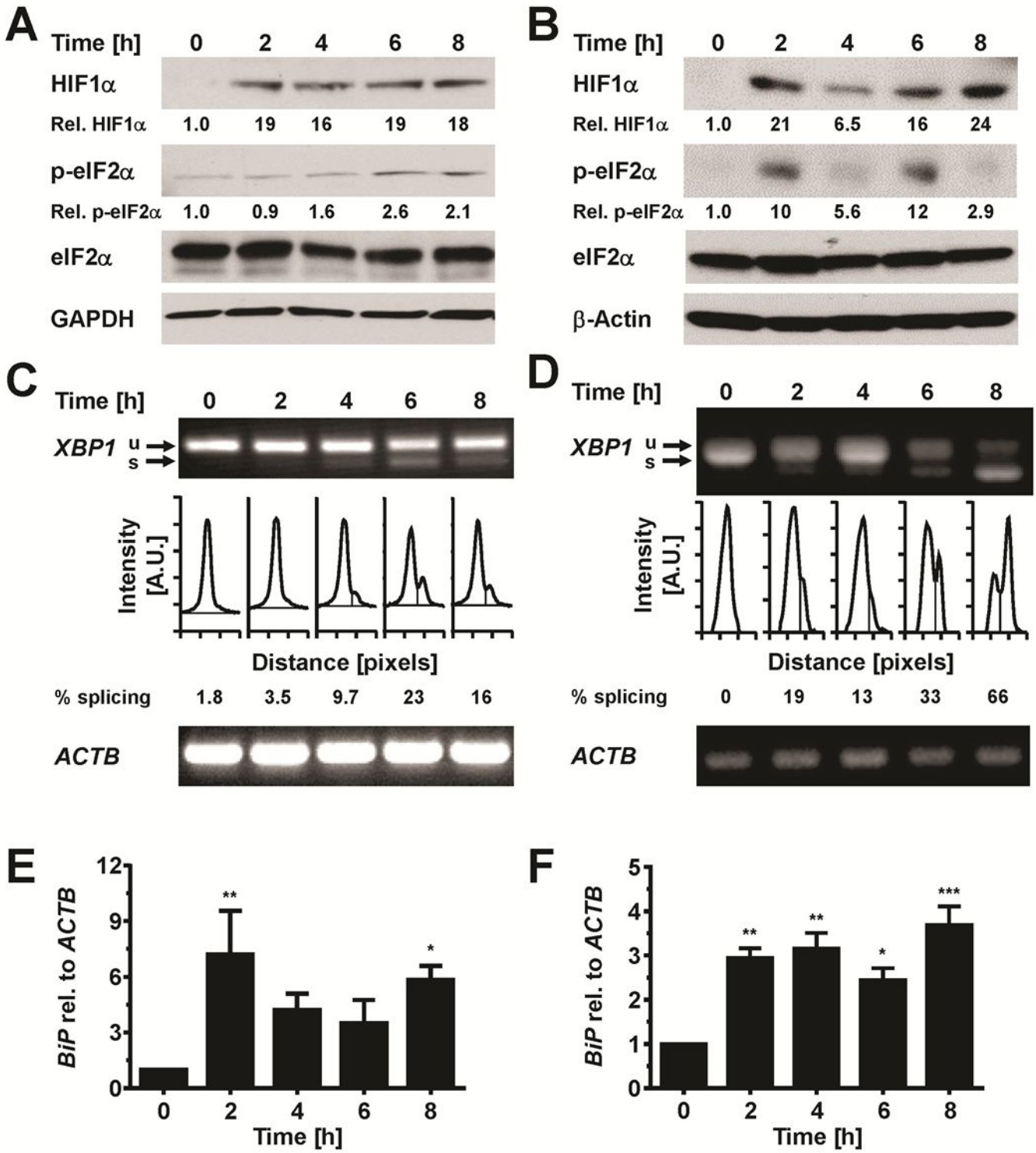

Mihai and Schröder, Figure 9